19941228 104

TRACKING AND IMPACT PREDICTION OF

EARTH-CROSSING-OBJECTS (ECOs) ON A

COLLISION COURSE WITH EARTH

THESIS
Gregory Alan Bishop
Captain, USAF

AFIT/GSO/ENY/94D-01

DEPARTMENT OF THE AIR FORCE

AIR UNIVERSITY

AIR FORCE INSTITUTE OF TECHNOLOGY

Wright-Patterson Air Force Base, Ohio

AFIT/GSO/ENY/94D-01

DTIC
ELECTE
DEC 3 0 1994
F

TRACKING AND IMPACT PREDICTION OF

EARTH-CROSSING-OBJECTS (ECOs) ON A

COLLISION COURSE WITH EARTH

THESIS
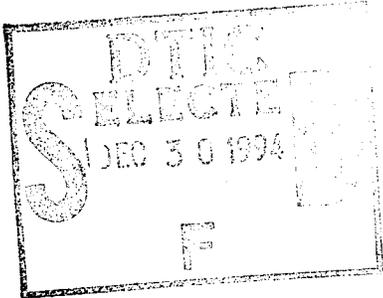Gregory Alan Bishop
Captain, USAF

AFIT/GSO/ENY/94D-01

Approved for public release; distribution unlimited

AFIT/GSO/ENY/94D-01

TRACKING AND IMPACT PREDICTION OF EARTH-CROSSING-OBJECTS
(ECOs) ON A COLLISION COURSE WITH EARTH

THESIS

Presented to the Faculty of the Graduate School of Engineering

of the Air Force Institute of Technology

Air University

In Partial Fulfillment of the

Requirements for the Degree of

Master of Science in Space Operations

Gregory A. Bishop, B.S.

Captain, USAF

NOVEMBER, 1994

ACKNOWLEDGMENTS

Table of Contents

List of Figures

List of Tables

ABSTRACT

This study investigated the effectiveness of Earth-based angles only observations in determining the orbit of various hypothetical Earth-Crossing-Objects (ECOs). "True" trajectories were simulated specifically for Earth-Crossing-Comets (ECCs) by numerically integrating in a Restricted Three Body system. Starting at Earth impact points, the state vectors were "reverse-propagated" to a proposed detection time. Observations (obs), with state-of-the-art accuracy, were then simulated with error induced by a Gaussian random number generator; these were used in a least-squares differential corrector to estimate the positions of the ECOs. State vectors and covariance matrices were then propagated to the impact times and axis lengths of the one sigma impact footprint were calculated. Varied amounts of data were fed into the differential corrector and it was determined that Earth-based obs alone may be ineffective in predicting an ECC's orbit.

TRACKING AND IMPACT PREDICTION OF EARTH-CROSSING-OBJECTS (ECOs) ON A COLLISION COURSE WITH EARTH

I. Introduction

1.1 Background

The proposal of the theory in 1980 that a large asteroid impact caused the dinosaurs' extinction about 65 million years ago significantly increased public awareness of the threat to Earth, and mankind, posed by asteroids (3:141). Relatively small-scale efforts to bolster the detection rates of asteroids, which for years were seen as simply the "vermin of the skies" due to their intrusion on the photographic plates of astronomers looking for other heavenly bodies, were begun in earnest at about the same time (7:27). Some of these efforts included searches conducted at the Mt. Palomar observatory in California and Project Spacewatch, in Arizona which "pioneered the use of Charge-Coupled Devices (CCD's) for semi-automatic searches using computers" (7:3). These and other efforts worldwide, however, are simply not enough to "scratch the surface" in detecting the estimated 320,000 Near-Earth-Asteroids (NEAs) which are 100 m or greater in diameter (7:12).

This fact begs the question of whether we need to be concerned with asteroids which are this small or smaller. The answer to this question continues to be a topic of great debate among experts in the field. This was evident in two workshops that were conducted by NASA as a result of congressional direction received in 1990 to "define a program for dramatically increasing the detection rate of Earth-orbit-crossing asteroids . . . [and to] . . . define systems and technologies to alter the orbits of such asteroids or to destroy them if they should pose a danger to life on Earth" (8:3). The first, the NASA

International Near-Earth-Object (NEO) Detection Workshop, was conducted in several phases during 1991. The second, the Near-Earth-Object Interception Workshop, was held in January 1992 (5:2).

The major result of the NEO Detection Workshop, whose members hailed from six different countries, was to recommend a system of six 2-3 meter telescopes that would be located around the world and be dedicated to the discovery and cataloguing of NEOs. Such a system would represent a moderate investment, by the workshop's estimate. Its primary goal would be to detect and catalog 90% of the NEOs 1 km and greater in diameter. The workshop's conclusion was that it is asteroids and comets of this size which represent the greater hazard to Earth due to the potential for damage on a global scale. Smaller objects, 100 m to 1 km in diameter, which hit the Earth with much greater frequency and could cause hundreds of thousands of casualties or more, would be detected but not at a level which would approach completeness. However, the Spaceguard Survey, which was the report produced from the workshop, admitted that ". . . some people consider the threat of the more frequent Tunguska-like events to be more relevant to their concerns . . ." (8:13). The Tunguska event was an impact by an asteroid or comet, in 1908, which was estimated to be about 80 m in diameter. It impacted in Siberia, causing trees to be flattened and ignited out to a radius of about 40 km.

The argument as to which size range of NEOs represents the greatest threat will surely go on for years to come and until we have better data on the population distribution of all Earth-Crossing-Objects (ECOs). ECOs represent a subset of NEOs whose orbits actually intercept that of the Earth and therefore have the potential for colliding with Earth while in their present orbit. They include long-period-comets (lpcs), several classes of Earth-Crossing-Asteroids (ECAs), intermediate period comets (ipcs), and short period comets (spcs, which are usually grouped with ECAs since their numbers are small and their orbits similar). Although some researchers tend to focus more on the

asteroid threat, comets cannot be ignored. In fact, although they are fewer in number, comets (lpcs and ipcs at least) represent more of a threat from the standpoint of warning time. Because of their higher eccentricity and longer period, they spend less time in the Earth's vicinity and offer smaller and more infrequent windows for detection.

For the purposes of this thesis, Comet Shoemaker-Levy 9's break-up about two years ago and recent impact with Jupiter could not be more timely. This once-in-a-millennium event, which occurred between 16 and 22 July of this year, consisted of impacts by 21 major pieces of the comet. At least two of these were estimated to be two miles in diameter, with others as big as one-half mile; the largest pieces were seen by many amateur astronomers using telescopes as small as four inches in diameter (2:1). This is not surprising considering the blasts from the largest pieces of Shoemaker-Levy 9 were estimated to be "equivalent to 250 million megatons of TNT. (The largest hydrogen bomb ever detonated produced a blast equivalent to about 5 megatons)" (2:2). The visibility of this event, both through a telescope and through the media, has served to further pique the public's awareness of the dangers that ECOs pose.

Although scientists estimate a 1-in-10,000 chance of such an event happening on Earth in the next century, the consequences would be so catastrophic that the overall risk to individuals is at least as great as other natural disasters with which we are used to dealing (9:107). But beyond a quantitative analysis lies a real qualitative danger which makes this type of cataclysm more menacing than the others. It is this type of known disaster alone which has the potential for bringing about the complete annihilation of species, as likely occurred 65 million years ago. We may choose to invest in just enough "insurance" to avert this kind of globally threatening collision or we may choose to be prepared to save hundreds of thousands of lives by diverting a smaller object. Either way, we will need the capabilities necessary to affect the tracking and impact prediction of ECOs on a collision course with Earth.

1.2 Problem

The problem which the Earth, and therefore the United States, will face sometime in our future (be it tomorrow or 10,000 years from now) is that we must be able to track and possibly intercept an ECO which we have detected and suspect to be on an impact trajectory with Earth. Interception will be required if and when we determine that the ECO is large and dense enough to be a threat and can say with enough certainty that it will in fact impact the Earth. Furthermore, we may need to know to some degree of accuracy where on the surface of the Earth the ECO will impact.

1.3 Research Objective

The objective of this research is to determine how soon and how well we could determine the impact point of an Earth-Crossing-Comet (ECC) on an impact trajectory with Earth, assuming we have only recently detected such an ECC. ECCs will be examined since they represent the most difficult scenario. The question will be answered with assumed capabilities similar to optical systems which are now or could soon be available. This knowledge will be critical in the context of effecting an interception for ECOs which are indeed deemed a threat. Additionally, answers to these questions should allow us to better determine what actions can be taken short of interception to prepare for an impact (i.e. evacuation of a given area).

1.4 Scope of Research

This thesis is divided into five specific areas of research and analysis. The first is an analysis of the ECO population. This is done to present an overall picture and to emphasize the fundamentally different type of threat that ECCs represent. Secondly, an analysis of the optical system proposed by The Spaceguard Survey and presently available radar technology is made to determine what detection and tracking capabilities

1-4

are now, or could be soon, available. Third, "truth" models are developed for the Earth-Sun-ECC systems to be studied and observations are simulated. Following that, the ECCs' orbits are estimated. Lastly, the results are analyzed to determine how soon and how well we were able to estimate the impact points using the assumed capabilities.

1.4.1 Analysis of the ECO Population The purpose of this analysis is to review what is currently known about the population of NEOs and specifically ECOs. This will provide us with a threat assessment for given size ranges of ECOs and a basis for selecting hypothetical ECCs for our truth models. Specific questions which will be answered include:

- What are the orbits of the known ECOs?
- What is the size distribution of the ECO population?
- What is the expected frequency of impact for different size ranges?
- What is the estimated material make-up distribution?
- What is the expected damage from the given types of ECOs?

The answers to these questions and the results of the analysis will be presented in the Literature Review (Chapter II).

1.4.2 Analysis of Detection and Tracking Capabilities. Having established what is known about the ECO population to date, we should determine what our prospects are for increasing that knowledge and detecting an ECO on an impact trajectory with Earth. Specifically we will examine the following questions:

- What technologies exist to accomplish the mission?
- What systems exist or have been proposed?
- What are the possible scenarios for discovery and interception?

Again, these questions are analyzed and answered in the Literature Review (Chapter II).

1.4.3 Truth Model Development and Observation Simulation. The truth models will be developed according to the classic "Restricted Three-Body Problem." FORTRAN routines will generate "perfectly known" trajectories from which "perfect data" will be taken and observations (which emulate the assumed capabilities) simulated by using a Gaussian Random Noise generator.

1.4.4 Orbit Estimation. Here the simulated observations will be used to estimate the ECCs' orbits by means of a Least Squares algorithm.

1.4.5 Data Analysis. An analysis of the output from the Least Squares algorithm will be made to determine the state vector position errors at the impact points for the ECCs based on the given frequencies and spans of observations.

II. LITERATURE REVIEW

2.1 Introduction

The purpose of this chapter is to provide a review of literature and information pertinent to this research. The goal of the literature review was to lay the ground work for the research effort. The following subjects are covered in the review:

- Classes of ECOs.

- ECO population and discovery completeness.

- Frequency of impact, damage expectation, and risk assessment.

- Past, present, and future systems and technologies for detection and tracking.

- Possible scenarios for discovery and interception.

2.2 Classes of ECOs

ECOs are generally classified according to their orbit type. There are three established classes of ECAs: Aten, Amor, Apollo. Their orbits are depicted in Figures 2.1, 2.2 and 2.3 (5:17, 18). Comets, including lpcs, ipcs, and spcs, which are defined as having periods of less than 20 years, 20-200 years, and greater than 200 years, respectively, are "distinguished by astronomers on the basis of their telescopic appearance." Objects that appear to have some sort of atmosphere due to volatile materials such as water or ice being heated by the sun are termed comets; other objects which appear more "star-like" are called asteroids (8:15).

Aten asteroids are unique among these three classes because they have periods which are less than Earth's. They are specifically defined as asteroids which have semimajor axis less than 1.0 AU (an astronomical unit is the distance from the Earth to the Sun) and aphelion distances greater than 0.983 AU (8:B-1).

The remaining two types of ECAs have periods which exceed Earth's. Amor asteroids in particular are defined as having a perihelion distance between 1.017 and 1.3
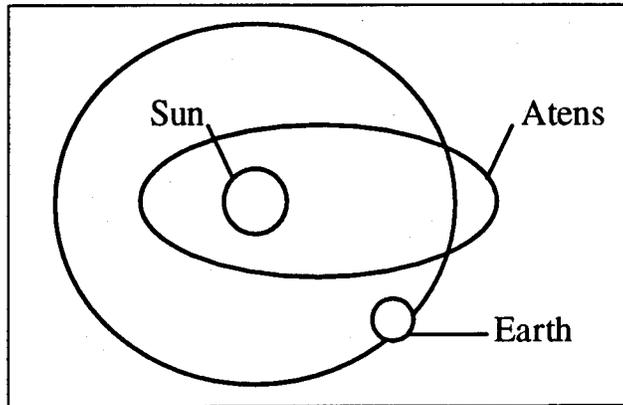
Figure 2.1 Orbits of Aten Asteroids (5:18)

AU and, for the most part, do not cross Earth's orbit, although some have been discovered which do.

Finally, the most cataloged type of ECAs are the Apollo asteroids which are defined as having semimajor axis greater than or equal to 1.0 AU and perihelion distances less than or equal to 1.017 AU (8:B-1).

Short period comets are often in orbits similar to Amor class asteroids, as can be seen in Figure 2.2. Lpcs and ipcs, on the other hand, typically have higher eccentricity orbits
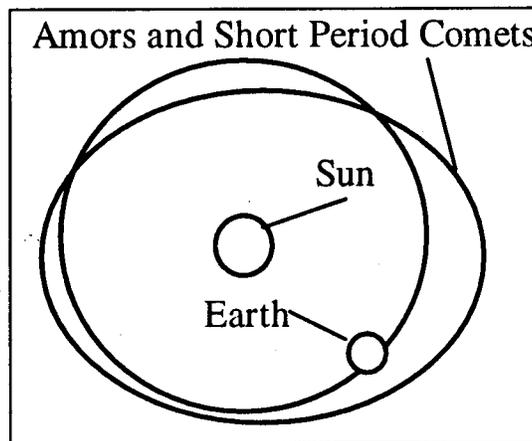
Figure 2.2 Orbits of Amor Asteroids and Short Period Comets (5:18)
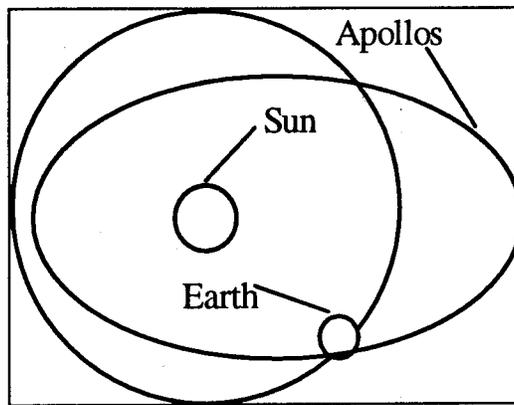
Figure 2.3 Orbits of Apollo Asteroids (5:17)

and are grouped together by some as ECCs; this is probably due to the fact that Amor type orbits, and therefore spcs, mostly due not intersect the Earth's orbit, as mentioned before. ECC orbits can be depicted as in Figure 2.4 (5:19).
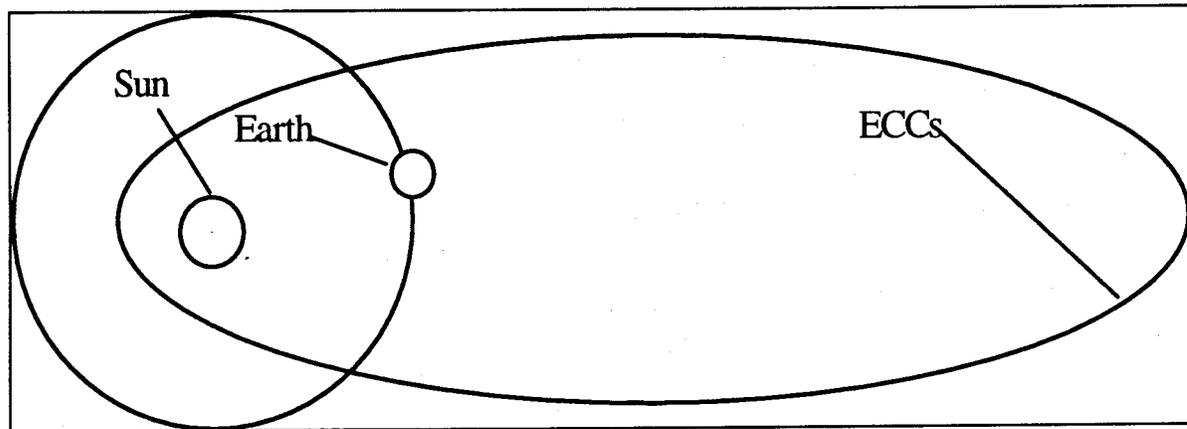
Figure 2.4 Orbits of ECCs (5:19)

2.3 ECO Population and Discovery Completeness

2.3.1 ECA and spc Population and Discovery Completeness.

As of the meeting of the Near Earth Object Detection Workshop in June 1991, the

total number of known ECAs was 128. These consisted of 11 Atens (9 percent), 85 Apollos (66 percent), and 32 Earth-Crossing Amors (25 percent) (8:15). By the beginning of 1992, this number had increased to 163 (4:34). Unfortunately, this number is by all estimates a mere "drop in the bucket" when we consider the total ECA population.

The Spaceguard Survey estimated the discovery completeness of ECAs as a function of absolute magnitude. Table 2.1 summarizes this information (8:15). "The absolute magnitude is defined as the apparent magnitude the object would have if it were 1 Astronomical Unit (AU), or 150 million kilometers, from both the Earth and Sun (8:15)." Also, lower and higher reflectivity is considered similar to C-class and S-class asteroids respectively.

Table 2.1 Discovery Completeness of ECAs

as a Function of Absolute Magnitude.

%Detected	Absolute Magnitude	Diameter (km)	Reflectivity
100%	13.5	14	lower
100%	13.5	7	higher
35%	15	6	lower
35%	15	3	higher
15%	16	4	lower
15%	16	2	higher
7%	17.7	2	lower
7%	17.7	1	higher

Compiled from (8:15)

The population of ECAs and comets may be estimated by use of a power law, as follows, where N is the number of ECAs, D is a given diameter, k a constant, and b the power law exponent:

$$N = kD^b \qquad (2\text{-}1)$$

Adopting values of b as -2.6 (D≤0.25 km), -2.0 (0.25 km <D≤2.5 km), and -4.3 (D>2.5 km) the spaceguard survey arrived at the estimates in Table 2.2 for the ECA population.

Table 2.2 Estimated ECA Population for Given Diameters

Diameter	Number of Asteroids
10 m	150 million
100 m	320,000
500 m	9,200
1 km	2,100
2 km	400

Compiled from (8:16)

The population estimates for spcs are as follows: 30±10 (D>1 km), 125±30 (D>0.5 km), 3000±1000 (D>0.1 km) (8:16). Comparing these numbers with those given above for ECAs it is evident that spcs number only about 1% of the total ECA population. Therefore, because of the error associated with ECA estimates, spcs may be considered as part of the ECA population for numerical estimates (8:16).

2.3.2 ECC Population and Discovery Completeness. Defining ECCs as having a period greater than 20 years and a perihelion less than 1.017 AU, an estimated 3 ECCs, with absolute magnitude of 10.5 (3-8 km in diameter) per year cross Earth's orbit. For ECCs above 1 km in diameter, The Spaceguard Survey estimated 100 per year pass within Earth's orbit (8:28). Also, because of the long periods involved, during the proposed 25-year survey most lpcs will only offer at most one opportunity for detection; therefore, the best we can hope for is to detect them with the greatest amount of warning time possible. Finally, from their orbital and size distributions, the total number of ECCs is estimated to be about five times the number of Earth-crossing spcs or 5 to 10 percent of the ECA population. But because of higher impact velocities (on the order of 60 km/sec)

and larger diameters they are estimated to comprise about 25 percent of the total NEO hazard (8:16). Additionally, impacts from lpcs could occur from any direction.

It is evident from the data presented above that we have a long way to go towards discovering and cataloging ECOs. Although the discovery rate for ECOs has increased dramatically over the last ten years or so, any comprehensive knowledge regarding the true ECO population can only come about through a systematic and dedicated effort. A system like the one proposed in The Spaceguard Survey would be a good first step but the question remains as to whether it would provide the necessary completeness for ECO defense.

2.4 Frequency of Impact, Damage Expectation, and Risk Assessment

2.4.1 ECO Categories. In the context of this section it is useful to define three categories of ECOs:

- Category 1 (10 m - 100 m diameter) - Impacting body generally is disrupted before it reaches the surface; most of its kinetic energy is dissipated in the atmosphere, resulting chiefly in local effects.

- Category 2 (100 m - 1 km diameter) - Impacting body reaches ground sufficiently intact to make a crater; effects are still chiefly local although nitric oxide and dust can be carried large distances, and there may be a tsunami if the impact is in the ocean.

- Category 3 (1 km and above) - Large crater-forming impact generates sufficient globally dispersed dust to produce a significant, short-term change in climate worldwide, in addition to devastating blast effects in the region of impact.

The diameters given above, however, serve only as guidelines, since any particular ECO cannot be placed into one of the categories without considering its density, strength, and velocity (8:8).

Table 2.3 Assessments of the NEA Population with Estimates of Impact Frequency for a Range of Asteroid Sizes.

NEA Population		Frequency of Collision (years)	
Diameter (m)	Number	Spaceguard	Steel
10	150 million	10	1
100	320,000	2,000	500
1,000	2,100	200,000	70,000
10,000	1	100,000,000	100,000,000

Compiled from (7:12)

2.4.2. Frequency of Impact. Methods vary for determining frequencies of impact and estimates rely on the population statistics used. Table 2.3 presents results for NEAs from The Spaceguard Survey and calculations conducted by Duncan Olsson-Steel in 1990 (7:12).

2.4.3. Damage Expectation. We can characterize damage expectation by examining the categories defined above and the material compositions of ECOs.

2.4.3.1. Material Compositions of ECOs. Material compositions of . ECOs do vary. Asteroids can be either soft stone, hard stone, or nickel-iron (6:1119). Comets on the other hand can be characterized as "dustballs or fluff" upon impact due to their volatiles being removed (6:1119). An estimated 95 percent of meteorites (meteoroids surviving the atmosphere) are soft stony objects (6:1132).

2.4.3.2. Category 1 Impacts. For ECOs on the order of 10 m in diameter, "only rare iron or stony-iron projectiles reach the ground with a sufficient fraction of their entry velocity to produce craters" (8:8). Typically, stony ECOs are crushed and fragmented as they are decelerated in the atmosphere to free-fall velocity.

Their kinetic energy is transferred to an atmospheric shock wave whose energy is divided between the "meteoric fireball" (characterized as a burst of light and heat) and a mechanical wave. Usually disruptions in this size range occur high enough in the atmosphere so that no damage occurs on the ground. For larger impactors in this category, however, damage on the ground is a possibility. The blast waves from soft stony meteorites, for example, are expected to cause ground damage if their diameter exceeds about 56 m (6:1132). For instance, the impact of a 68 m diameter stony asteroid traveling at 20-25 km/s would cause ground damage over an area the size of Chicago (6:1132). This ominous calculation is tempered with the estimate that the average interval between impacts for world urban areas is 100,000 years with the corresponding interval for populated areas of Earth being 3,000 years (3:55).

Probably the most cited such event occurred in 1908 over the Tunguska region in Siberia. This impactor was estimated to be anywhere from 60 to 80 m in diameter and to have released energy on the order of 12 to 20 (possibly as high as 48 [6:1132]) megatons, depending on the data source (8:8). Regardless of the exact size and energy, the results were that "Siberian forest trees were mostly knocked to the ground out to distances of about 20 km from the endpoint of the fireball trajectory, and some were snapped off or knocked over at distances as great as 40 km" (8:9). Additionally, some evidence indicates that fires were ignited out to a distance of 15 km (8:9). Should an impact like this occur over an urban area, buildings would be flatted and fires ignited; the results would resemble a nuclear explosion, except for the lack of radiation, with casualty estimates in the hundreds of thousands (7:9).

Ground damage occurs for nickel-iron meteoroids at a much smaller diameter than for stony objects; nickel-iron meteoroids traveling at 11.2 km/s (the lowest parabolic velocity for an object hitting Earth) produce ground damage if their diameter exceeds 4 m.

Comets, on the other hand, cause ground damage when traveling at 40 km/s only if their diameter exceeds 100 m. Regardless of the make-up of the ECO, ground damage on the order of that described above occurs whenever "the over pressure in the blast wave exceeds 4 pounds/inch^2" (6:1114).

      2.4.3.3. Category 2 Impacts. Category 2 impacts represent, of course, a greater hazard. They could reach the ground intact and form a crater; evidence and theory suggest that the cut-off size for stony objects to produce cratering is 150 m in diameter (8:9). However, as counterintuitive as it may seem, impactors which barely survive the atmosphere will impart much of their energy to the ground and thus may not cause any greater damage than smaller ECOs which cause air bursts (8:9). It is the upper end of Category 2 objects which represent a somewhat unknown, and surely greater hazard, since their energies would dwarf those of nuclear explosions studied to date. Damage for 1 km events is expected to cover entire states or countries "with fatalities in the tens of millions in a densely populated region" (8:9).

"If the impactor produces a crater, it must produce an earthquake" (6:1140). Although most of an impactor's energy goes into producing the crater, for Category 2 objects and above the magnitude of the earthquake can still be significant. In fact, a stony asteroid with a diameter of 520 m and an impact velocity of 20 km/s "produces an earthquake of Richter scale 8.8, which equals that of the largest earthquake ever recorded" (6:1142). If similar impacts occur in the ocean the results are deep water waves which produce tsunamis. "Because a disproportionate fraction of human resources are close to the coasts, tsunamis are probably the most deadly manifestations of asteroid impacts apart from the very large Cretaceous-Tertiary superkillers [the size impact which is hypothesized to have caused the dinosaurs' extinction]" (6:1142). A 400 m diameter asteroid which fell in the Atlantic Ocean would produce a tsunami over 200 m high lasting

at least 2 minutes on both the North American and the European coasts (6:1142).

It is notable that comets up to even 1 km may not survive the atmosphere intact due to their composition of mostly water ice and other volatiles (8:9). Comets, however, offer some different types of dangers. For instance, they start fires much more readily than asteroids (6:1134). Because they dissipate their energy higher in the atmosphere, they illuminate a larger area on the surface and their atmospheric shock waves do not reach the surface as easily. This means that fires which are ignited are not immediately extinguished, as often happens with asteroids.

2.4.3.4. Category 3 Impacts. Category 3 impacts represent the greatest potential hazard because objects in this size range are large enough to produce global damage. The exact diameter beyond which global effects occur is still a matter of debate, but estimates place it between 0.5 and 5 km, perhaps near 2 km (8:11). The greatest hazard from impactors in this size comes from the veil of dust and debris which would be injected into the atmosphere as a result of the crater produced. Crater sizes here are expected to be "10 to 15 times the diameter of the projectile (8:9)." This veil would block the Sun and, with increasing amounts of dust injected, cause crop failures and mass mortality (8:9). If the impactor were large enough, the survival of civilization and even the human species would be at risk. The Cretaceous-Tertiary impactor is an example of this size ECO; it is estimated that it was about 10 km in diameter (7:6). Additionally, since this impact did produce widespread fires, experts suggest that it was a comet (6:1135).

2.4.3.5. Impact Energies. As alluded to earlier, another common way to analyze the damage potential of ECOs is to calculate impact energies in terms of megatons of TNT. Table 2.4 cites impact energies for asteroids of different size ranges in terms of

ergs, megatons TNT, and number of Hiroshima-equivalent explosions. These energies assume impact velocities of 20 km/sec (7:13).

Table 2.4 Asteroid Impact Energies.

Asteroid Impact Energies				
Diameter (m)	Mass (kg)	Ergs	Hiroshimas	Megatons TNT
10	2×10^6	4×10^{21}	7	0.1
100	2×10^9	4×10^{24}	7000	100
1000	2×10^{12}	4×10^{27}	7,000,000	100,000
10000	2×10^{15}	4×10^{30}	7×10^9	100,000,000

Compiled from (7:13)

2.4.4. Risk Assessment. It is in the realm of risk assessment that the greatest amount of dissension among experts occurs. Due to uncertainties about the exact population distribution of ECOs, impact frequencies, and damage expectation, the ECO size which represents the greatest risk is a matter of controversy. Preliminary results from the Spacewatch Program indicate that the number of 50 to 100 m objects may be greater than previously estimated. If this is the case "and if the threshold for global catastrophe is near the upper end of the range of uncertainties, then the annualized risk of fatalities might actually be dominated by Tunguska-class impactors" (3:293). Some believe, however, that even if the numerical hazard is greatest among the Tunguska-class, we should still be more concerned with globally catastrophic impactors since it is this type of catastrophe alone which could cause the end of our civilization or our species. Regardless of which size ECO represents the greatest hazard, the overall risk from an ECO impact is probably higher than most expect, considering the relative infrequency of impact. However, if we combine the low frequency of impact and high mortality estimates, the resulting overall risk is on the order of other risks which we are more familiar with (see Table 2.5).

Table 2.5 Risk Assessment.

Threats: A Comparison	
Estimated Risk for an American over a 50-year period	
Risk of death from botulism	1 in 2,000,000
Risk of death from fireworks	1 in 1,000,000
Risk of death from tornadoes	1 in 50,000
Risk of death from airplane crash	1 in 20,000
Risk of death from asteroid impact	**1 in 6,000**
Risk of death from electrocution	1 in 5,000
Risk of death from firearms accident	1 in 2,000
Risk of death from homicide	1 in 300
Risk of death from automobile accident	1 in 100

Compiled from (7:15)

2.5. Past, Present, and Future Systems and Technologies.

2.5.1. Past and Present Efforts. As stated earlier, there have been only about 200 NEOs discovered to date; this is a very small fraction of the hundreds of thousands which exist in sizes of 100m and greater. "Over two thirds of the known near-Earth asteroids have been found in the last fifteen years" (7:3). This is due in part to a lack of interest in detecting asteroids. Astronomers have in the past seen asteroids as a nuisance because they interfered with their efforts to observe other objects in the sky. Most of the early asteroids were discovered while astronomers were using photographic plates to capture stellar images. This technique was pioneered in Heidelberg, Germany, early in this century (7:26). "One German astronomer even referred to asteroids as the 'vermin of the skies'" (7:27). This attitude led to many plates being thrown away because they had been "ruined by an ugly streak" (7:27).

In more recent years many asteroids have been discovered by supplementing the photographic plate method with two major techniques. The first is to take two consecutive 10-20 minute exposures of the sky where the telescope moves at the same rate as the stars. Asteroids then appear as streaks, the length and direction of which help to determine orbital parameters. A second technique is to take photographs about 45 minutes apart. The plates are examined using a stereo microscope; the objects that have moved stand out relative to the star field. This technique allows shorter exposure times and has resulted in greater sky coverage in recent years. Its drawback is that larger telescopes cannot be used because their plates "are too large to be viewed through a stereo microscope" (7:31).

A one-time detection, however, is usually insufficient to allow reacquisition of an asteroid other than immediately following such detection. Consequently, it is extremely important for a newly detected asteroid to be reacquired in short order so accurate orbital parameters may be calculated (7:32). This frequently does not occur due to inadequate cooperation; "time on large telescopes is in high demand and is usually allotted well in advance" (7:32).

One relatively recent advance which significantly improves NEA detection rates is the Charge-Coupled Device (CCD). It is "a solid state chip containing an array of photoelectrically sensitive pixels in a grid-like pattern. Placed on the focal plane of a telescope, this device traps incoming photons, converting them into electrons. Each pixel is also a tiny capacitor which can hold a charge until it is given the command to move it, at which point the pixels are shifted row by row to the edge of the chip, where they are read

in by a computer (7:34)." The major advantages are greater sensitivity and bandwidth, automation, and real-time processing. "Real-time processing means that no time is lost between the actual observation and the discovery so that follow up observations can proceed immediately. The presence of the computer also allows more exact measurements as well as automatic calculation of orbital parameters and future positions" (7:36). Drawbacks to CCD technology include fragile equipment (which must be cooled with liquid nitrogen) and significant maintenance with relatively few qualified people to conduct it (0:36). CCD technology is expected to advance, however, and "will certainly come to dominate the field of astronomy" (7:37).

One military program, Ground-based Electro-Optical Deep Space Surveillance (GEODSS), which was developed in the 1980s for the Air Force, is considered to be "ideally suited for NEA search work" (7:38). "In the period from 1980-1984, ... MIT Lincoln Laboratory adopted the first of these telescopes [the one located at Socorro, N.M.] for asteroid observation and used it to conduct a systematic search. A discovery rate of 25 NEAs per year was predicted for the system, but in fact none were found, though several main-belt asteroids were reported" (7:38). No explanation was found during this research to clarify this unexpected result.

Current space-based systems have contributed to detection of NEAs. These systems have the advantage of avoiding atmospheric distortion, so that fainter objects may be detected. Their major disadvantage is expense. No system has been developed which is exclusively dedicated to NEA detection.

The Infrared Astronomical Satellite (IRAS) launched in 1983 did conduct asteroid

observations which "constitute 'the largest, most complete and least biased survey of asteroids and comets yet conducted'" (7:43). This result was obtained even though some instruments on the IRAS did not function properly.

Other space-based systems which have the potential to contribute or have already contributed to NEA detection include the Hubble Space Telescope (HST), European Space Agency's (ESA) Hipparcos, and the planned Space Infrared Telescope Facility (SIRTF). The HST "has considerable potential . . .[but] . . . time for the HST is extremely hard to come by . . .". Hipparcos, launched in 1989, ". . . is providing observations of substantially higher accuracy than have ever been achieved before, but is somewhat limited in that it can only view relatively bright objects". SIRTF offers the advantage that "it conducts its observations in the infrared band [and] it is not dependent on reflected sunlight for observations". However, this system already "suffers from time oversubscription,... and [as of December 1992] has not yet even been launched" (7:43).

2.5.2. Future Efforts. One can see that the technology exists to conduct extensive ground based and/or space based NEA detection efforts. The limiting factors seem to be the lack of systems which are dedicated to NEA searches and the financial resources necessary to establish them. The Spaceguard Survey addressed these issues.

2.5.2.1. The Spaceguard Survey Network. The proposed Spaceguard . Survey network would include "six 2.5 m aperture, f/2 prime focus reflecting telescopes, each with four 2048x2048 charge-coupled-device (CCD) chips in the focal plane" (8:vi);

2-15

these "would be placed around the world in both hemispheres so as to over as large a portion of the celestial sphere as possible . . . " (7:61). It is expected that 90 percent of all ECAs greater than 1 km in diameter would be discovered in the first 25 years of operation; a dark-sky survey (defined below) would detect most lpcs several months before approaching Earth. Others could be detected with significantly less warning time, as we will see. "Tens of thousands of smaller asteroids (down to a few meters in diameter)" would also be discovered, but the completeness of the survey declines significantly for objects under 500 m in diameter (8:vi). In fact, the estimates are that two-thirds of NEAs larger than 500m in diameter, and about a tenth of the asteroids over 100m in diameter (based on implementation of its "standard survey") would be detected in the same time frame. The Spaceguard telescopes would be supported by back up telescopes and possibly a dedicated radar. Costs of the program are estimated at an initial $50 million in capital investment with annual operation expenses of $10 to $15 million" (7:61).

More detailed estimates of the expected discovery completeness were also given in The Spaceguard Survey. These estimates varied according to which of several search strategies was employed. The strategies examined were a whole-sky, dark sky, and standard survey. The whole-sky survey was deemed unrealistic, while the latter two were felt to be practicable. Present here are the results of the dark-sky survey estimates since it is the most comprehensive yet attainable search strategy; it assumes a search of ±120 degrees celestial longitude from opposition (opposite the direction toward the Sun) and ±90 degrees celestial latitude. Note, however, that the The Spaceguard Survey actually recommended implementing a network using the standard survey which would produce somewhat lesser results. Tables 2.3 and 2.4 include percent discovery completeness estimates for ECAs and ECCs, respectively, for searches conducted at two different visual magnitudes (V). For reference, V=22 searches detect somewhat fainter objects than those detected by the Spacewatch Telescope mentioned in Chapter 1. The ECA results, Table

Table 2.6 Dark-Sky Survey Simulations for ECAs (see text for details). The table gives percentage discovery completeness for both entire population and potentially hazardous ECAs larger than a given diameter.

Diameter	V=22		V=24	
50 m	3	5	16	25
0.1 km	12	19	42	55
0.5 km	76	84	97	98
1.0 km	95	96	99	99

Compiled from (8:31)

2.6, include estimates for all ECAs (column 1) and for a subset denoted as potentially hazardous (column 2); these are defined as "those that can come within about 0.05 AU, or about 20 times the distance to the Moon" (8:27). It is clear from these results that even if we choose to implement The Spaceguard Survey network, there is a distinct possibility that the Earth could be hit by an ECO without any warning. This possibility is obviously greater for smaller diameter ECOs that could do local damage, but note that for ECCs, using a system which detects objects at V=22, some 15 percent of the objects greater than 1 km would never be detected.

2.5.2.2. Criticisms of The Spaceguard Survey Network.

2.5.2.2.1. Survey Completeness. The Spaceguard Survey has been generally well received by the scientific community as an excellent response to the tasking by Congress. Its recommendations seem reasonable at first inspection. However, as demonstrated earlier, the damage potential is great for impactors in the size range of 100m to 1km in diameter, although possibly not on a global scale. The position

taken by the Spaceguard Survey on this size range of asteroids is as follows:

> Impacts by these bodies are below the energy threshold for
> global environmental damage, and they therefore constitute
> a smaller hazard in spite of their more frequent occurrence.
> Unlike the large objects, they do not pose a danger to
> civilization. (7:62)

This statement assumes that the global catastrophe threshold does lie above objects 1km in
diameter, which may or may not be true. If it is true, then the statement is valid but it
sidesteps the issue of the "smaller hazard," as does the recommended Spaceguard Survey

**Table 2.7 Dark-Sky Survey Simulations for ECCs (see text). The percentages for
zero warning time correspond to the overall discovery completeness.**

D>	Warning Time	% ECCs discovered	
(km)	(yr)	V=22	V=24
0.5	0	67	88
	0.25	54	83
	0.5	26	66
	1	5	16
1	0	85	94
	0.25	77	92
	0.5	59	84
	1	12	49
5	0	95	96
	0.25	93	95
	0.5	87	90
	1	68	79
	2	7	25
10	0	96	97
	0.5	90	93
	1	74	88
	2	18	74
	3	6	27

Compiled from (8:31)

2-18

Network. We cannot assume that, as a civilization, we are resigned to accepting, the risk of lesser catastrophes. The general population, may not be willing to resign themselves to this. Some would contend that it is not feasible to conduct a comprehensive survey of the skies that would provide warning with some certainty of an impact from one of the projected hundreds of thousands of objects in the 100m range. There are some studies being conducted which may indicate otherwise.

2.5.2.2.2. Radar Observations. According to the Spaceguard Survey:

> A single radar detection yields astrometry with a fractional
> precision that is several hundred times better than that of
> optical astrometry, so the inclusion of radar data with the
> optical data in the orbit solution can quickly and
> dramatically reduce the future ephemeris uncertainty
> (8:37).

Certainly no one would dispute this statement. In fact research indicates that, for asteroids and comets which have short intervals of optical data, "the addition of only a few radar observations allows a far more accurate extrapolation of their future motions" (16:303). The problem lies in acquiring these very important radar observations. There are two main obstacles to overcome in order to do this.

First, there are operational and budgetary concerns. The Spaceguard Survey indicates with regard to follow-up observations:

> As noted previously in this Report, it would be desirable to
> have one or more dedicated planetary radars and large-
> aperture optical telescopes (4-m class). However, we
> anticipate that a great deal of useful work could be done
> initially using existing planetary radars and optical facilities.
> Therefore, for the purposes of this Report, we simply

allocate a sum of $2 million per year for the support of
radar and optical observing on these instruments (7:64).

Others have pointed out that to "dismiss the network of follow-up telescopes by allocation

of a small amount of funds...seems short-sighted, and may conceal considerable later

expenses . . . " (7:64). Additionally, "radar installations on the scale of the Arecibo

installation do not come cheap, nor do 4 m aperture telescopes" (7:64). Lastly, if radar

observations are to be used as a routine follow-up for the expected 500 NEOs that will be

discovered per month, certainly relying on existing resources to handle that much "traffic"

is impractical.

On the other hand, borrowing radar resources to obtain observations only for ECOs

that we suspect may be on an impact trajectory is manageable from an operational and

budgetary perspective. However, even the most powerful radars in existence today have a

very limited range in this context. With current radars offering a range of 0.1 AU, radar

observations for ipcs or lpcs traveling at 60 km/sec on a collision course could only be

obtained within a few days of impact (3:31). This would offer little time for interception.

Obviously, we will need to determine whether or not a threatening ECO will impact

sooner. Radars with twice the current range could be built, and research indicates that "a

5- to 10-MW, 94-Ghz free electron laser (FEL) with a 15- to 50-m antenna could track

objects at about 1 AU" (3:210). Even if we could develop a 1 AU tracking ability, it is

desirable that we be able to predict an impact at even greater distances. The question is

then, wheter we can accomplish this with angles-only observations.

2.5.2.3. Space-Based Detection.

2.5.2.3.1. Earth Orbiting Scanner. The Naval Research .

Laboratory submitted a report in January of 1993 which considered the use of a space

based system to provide warning of asteroid impacts down to the 50m diameter size range. This study considered the use of infrared and visible systems. Its conclusion was that "although asteroid detection in the IR is possible, the warning time (assuming an asteroid radial velocity of 3 km/sec) associated with small asteroids is not sufficient to deploy countermeasures" (10:2). The recommendation of the report was to use "a satellite-borne visible scanner . . . to continuously monitor the celestial sphere for near Earth asteroids. The proposed scanner uses the parallax motion of near Earth objects against a fixed background of distant objects. Image processing techniques will allow the detection of asteroids as small as 50m in diameter at distances greater than 7×10^6 km [almost 0.5 AU]. This will give sufficient warning time against Earth intersecting asteroids" (10:i).

2.5.2.3.2. Surveillance From Heliocentric Orbit. "Long-period

comets on collision courses with the earth spend an inordinate amount of the previous year at small angular elongations from the sun" (3:69). In order to detect comets in this vicinity a system needs to be able to detect objects 100 times fainter than the proposed Spaceguard Network (3:69). Infrared systems have been proposed as a possibility for fulfilling this need, but analysis of IRAS data indicates that any objects which it detected could have also been detected with ground based optical telescopes and that the accuracy of the data was at least 20 times worse than optical telescopes (3:69). In order to achieve early detection of lpcs or NEAs with aphelia slightly outside of Earth's orbit (such as Aten asteroids) optical telescopes located far from Earth are recommended (3:69). It has been suggested that they be placed in a heliocentric orbit closer to the sun (or perhaps around Venus) (3:69).

2.6. Possible Scenarios For Discovery and Interception.

2.6.1. ECO Threat Categories.
ECOs can be categorized for threat according to the amount of warning time afforded by their detection and orbit determination. The following is one such categorization (5:22):

- Well Defined Orbits - have warning times on the order of decades (ECAs).

- Uncertain Orbits - have warning times on the order of years (Newly discovered ECAs and Short-Period Comets).

- Immediate Threat - have warning times on the order of 1-12 months (lpcs and small ECAs).

- No Warning - have warning times on the order of 0-30 days (lpcs and unknown ECAs).

2.6.2. Interception Scenarios.
Examining the categories above we can deduce that there are really two possible intercept scenarios, distant and close-in. A distant intercept scenario is, of course, preferable for numerous reasons. It requires much less change in velocity (delta-v) to accomplish the mission since intercepts would typically occur at ECO perihelion two or more orbits prior to the predicted impact orbit. This is the most efficient point to deflect an ECO. This would allow a "deflect-look-deflect" approach using much smaller deflection velocities (on the order of centimeters per second) and would allow any fragmentation to disperse before approaching Earth (5:21).

Close-in intercepts on the other hand offer a much more challenging scenario. Intercepts "would likely occur a few tenths of an AU from Earth and require deflections on the order of a thousand times larger than the distant intercept case" (5:21). These facts cause a requirement for high energy propulsion and deflection technologies that increase

the risk of fragmentation. Additionally, time may only allow one or two deflection

attempts (5:21).

III. Methodology

To analyze the effectiveness of angles-only observations (optical telescope obs which do not include range or range-rate information) in predicting the orbit and impact of ECOs on a collision course with Earth, the classical restricted three-body system has been chosen to model the orbits of ECCs. ECCs were chosen as a test case since they represent the most challenging scenario for detection, tracking, and interception. Also, since virtually all comets have not been discovered and have such long periods, even the proposed Spaceguard system could not develop a complete catalog.

3.1 The Restricted Three-Body Problem

First defined by Leonard Euler in 1772 during his research on the motion of the moon, the restricted three-body problem involves two primary bodies in circular orbits about their center of mass (12:266). A third body, whose mass is negligible with respect to the primaries, is introduced into the system. In this case, the primaries are the Earth and the Sun with the third object being a hypothetical ECC. The effects of other bodies in the solar system and any outgassing from the ECC are neglected. These may or may not be valid assumptions for any particular comet and trajectory.

3.1.1 Equations of Motion.
The equations of motion presented here conform to the convention which has grown around the study of the restricted three-body problem over the past 200 years. The convention involves the choice of units for mass, length, and time and for coordinate frames. The unit of length is taken as the distance between the two primaries, the Sun and the Earth, (12:267):

$$a_{12} = 1 \qquad\qquad (3\text{-}1)$$

Since the mass of the third body is neglected, the unit of mass usually chosen is the sum of the masses of the primary bodies: $m_1 + m_2 = 1$. Setting the mass of the Earth $m_2 = \mu$, the masses of the Sun and Earth are, respectively (12:267):

$$m_1 = 1 - \mu \tag{3-2}$$

and

$$m_2 = \mu \tag{3-3}$$
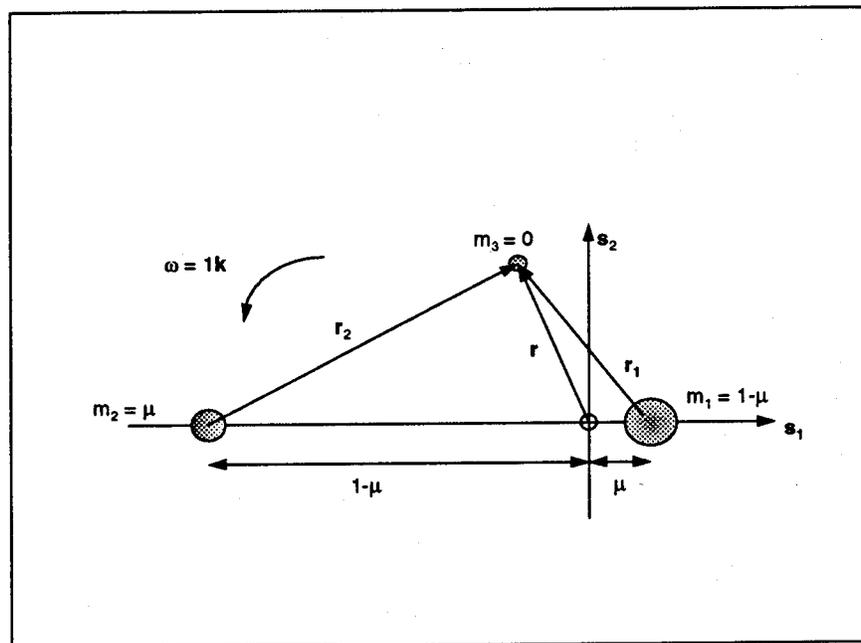
Figure 3.1. Geometry of the Restricted Problem. (12:268).

The unit of time is chosen so that the gravitational constant $G = 1$. This results in the period of the Earth and Sun in their orbits about each other to be, by Kepler's third law (12:267):

$$T_{12} = 2\pi \left[\frac{a_{12}^{\;3}}{G(m_1 + m_2)} \right]^{\frac{1}{2}} = 2\pi \tag{3-4}$$

The reference frame is rotating, again as is the convention, with its origin at the center of mass of the Earth-Sun system. The Earth and Sun lie on the s_1 axis with the Sun located at a distance $\mu = 0.0000030359$ (11:225). Since the restricted three-body problem uses dimensionless units, *"anything* can be measured in terms of μ" (12:268).

Now we can calculate the inertial acceleration of m_3, or the hypothetical ECC. Since we are in a rotating reference frame with angular velocity $\omega = 1\mathbf{k}$, applying Newton's second law yields (12:268):

$$\frac{{}^i d^2}{dt^2}\mathbf{r} + 2\omega \times \frac{{}^s d}{dt}\mathbf{r} + \omega \times (\omega \times \mathbf{r}) \qquad (3\text{-}5)$$

where the position vector of the ECC is (12:268):

$$\mathbf{r} = x\mathbf{s}_1 + y\mathbf{s}_2 + z\mathbf{s}_3 \qquad (3\text{-}6)$$

The time derivatives of Equation (3-5) in the rotating frame are (12:268):

$$\frac{{}^s d}{dt}\mathbf{r} = \dot{x}\mathbf{s}_1 + \dot{y}\mathbf{s}_2 + \dot{z}\mathbf{s}_3 \qquad (3\text{-}7)$$

and

$$\frac{{}^s d^2}{dt}\mathbf{r} = \ddot{x}\mathbf{s}_1 + \ddot{y}\mathbf{s}_2 + \ddot{z}\mathbf{s}_3 \qquad (3\text{-}8)$$

Substituting Equations (3-6), (3-7), and (3-8) into (3-5) and carrying out the cross products, the inertial acceleration of the ECC becomes (12:269):

$$\frac{{}^i d^2\mathbf{r}}{dt^2} = (\ddot{x} - 2\dot{y} - x)\mathbf{s}_1 + (\ddot{y} + 2\dot{x} - y)\mathbf{s}_2 + \ddot{z}\mathbf{s}_3 \qquad (3\text{-}9)$$

We must also calculate the gravitational acceleration of the ECC due to the Earth and Sun system. To do this we need the distance between each primary and the ECC. They are for the Sun and Earth respectively (12:269):

$$r_1 = \left[(x - \mu)^2 + y^2 + z^2 \right]^{\frac{1}{2}}$$

(3-10)

and

$$r_2 = \left[(x + 1 - \mu)^2 + y^2 + z^2 \right]^{\frac{1}{2}}$$

(3-11)

The gravitational acceleration of the ECC is then (12:269):

$$\mathbf{a}_g = -\frac{(1-\mu)\mathbf{r}_1}{r_1^3} - \frac{\mu \mathbf{r}_2}{r_2^3}$$

(3-12)

Finally, equating the acceleration due to gravity and inertial acceleration of the ECC and breaking each term out according to its components $\mathbf{s}_1, \mathbf{s}_2,$ and $\mathbf{s}_3$, respectively, the equations of motion for the ECC are (12:269):

$$\ddot{x} - 2\dot{y} - x = \frac{(1-\mu)(x-\mu)}{r_1^3} - \frac{\mu(x+1-\mu)}{r_2^3}$$

(3-13)

$$\ddot{y} - 2\dot{x} - y = \frac{(1-\mu)y}{r_1^3} - \frac{\mu y}{r_2^3}$$

(3-14)

$$\ddot{z} = \frac{(1-\mu)z}{r_1^3} - \frac{\mu z}{r_2^3}$$

(3-15)

To date there is no closed form solution to these second-order, highly nonlinear, coupled ordinary differential equations, so a Haming numerical integration scheme is used to find the trajectories of each hypothetical ECC.

3.1.2 The Lagrangian Equilibrium Points. These points, named for the discoverer of these triangular points, will be important later in this work. ECO Detection Satellites could be placed at these stable points to provide better detection capabilities, particularly for ECOs spending a great deal of time at opposition, and to provide vantage points other than Earth's for tracking ECOs.
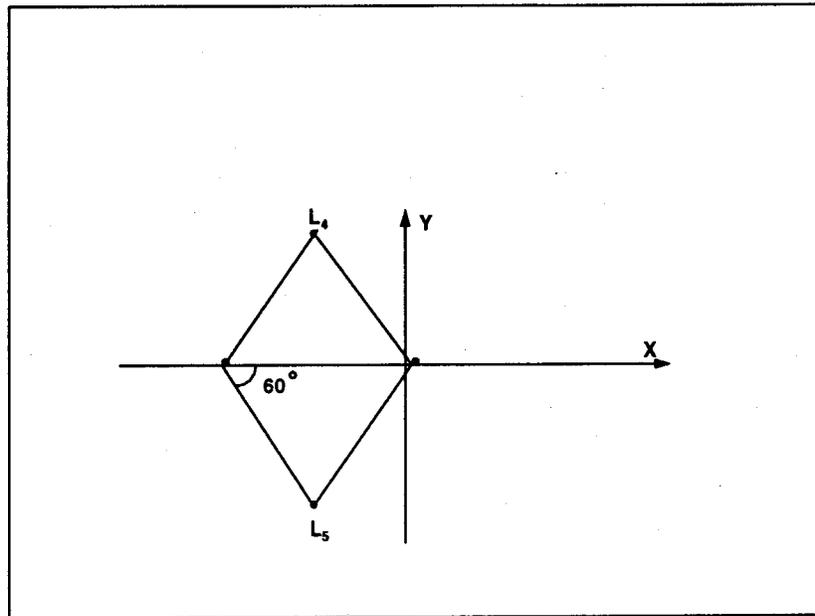
Figure 3.2. Lagrange Triangular Points. (12:271)

By setting the velocity and acceleration components to zero in the equations of motion for this system we find the following three equations (12:270):

$$-x = -\frac{(1-\mu)(x-\mu)}{r_1^3} - \frac{\mu(x+1-\mu)}{r_2^3}$$
(3-16)

3-5

$$-y = \frac{(1-\mu)y}{r_1^3} - \frac{\mu y}{r_2^3} \tag{3-17}$$

$$0 = \frac{(1-\mu)z}{r_1^3} - \frac{\mu z}{r_2^3} \tag{3-18}$$

Noting that, since $z = 0$, all Lagrangian Points must lie in the orbiting plane of the Earth-Sun system and setting $r_1 = r_2 = 1$, we find that the two equilibrium points with which we will be concerned lie at the vertices of equilateral triangles as pictured in Figure 3.2.

3.2 FORTRAN Program Library

This thesis relies upon the FORTRAN code developed by Dr. William E. Wiesel (13), which has been modified and supplemented with Dr. Wiesel's guidance. The main components of the program library include a "reality simulator," program Data, and a Least Squares Estimator, program Lstsq. Data accepts initial conditions and integrates them over a specified time using a Haming ordinary differential equations integrator. Lstsq, given an initial guess for the state vector, accepts observations (angles-only position data in this case) and using a non-linear least squares algorithm produces an estimate of the state vector at a specified time. The library consists of the following units:

- Program Data. Accepts initial conditions, integrates the equations of motion, and generates observations when used in conjunction with the subroutines listed.

- Subroutine Haming. Ordinary differential equations integrator.

- Subroutine Rhs. Calculates the state transition matrix.

- Subroutine Dynam. Contains restricted three-body equations of motion.

- Subroutine Obser. Calculates angles only observations.

- Function Randg. Gaussian pseudo random number generator.

- Function Rand. Gaussian pseudo random number generator.

- Subroutine Julday. Converts date and time information to modified Julian day.

- Program Lstsq. Nonlinear least squares algorithm.

- Subroutine Phpph. Propagates the covariance matrix.

- Subroutine Linv1f. Imsl-like matrix inverter.

- Subroutine Leqt2f. Performs Gaussian elimination with maximal pivoting.

- Subroutine Fotbal. Performs eigenanalysis of the covariance matrix.

- Subroutine Eigrf. Imsl-like eigenvalue routine.

- Subroutine Eigen. Generates eigenvalues of a real general matrix.

- Subroutine Compve. Finds complex eigenvectors corresponding to complex eigenvalues.

- Subroutine Hesqr. Finds all eigenvalues of a real general matrix.

- Subroutine Realve. Calculates real eigenvectors of matrix a in upper heisenberg form.

- Subroutine Escale. Scales a matrix and normalizes.

3.3 Truth Model Development and Observation Simulation

3.3.1 Setting Up the Impact Conditions.. In order to simulate an impact by an ECC an Earth impact point and velocity which met the characteristics of an lpc as found in the literature review were chosen. Impact velocities were all taken as 60 km/sec "straight in" or on a line parallel to the Earth's radius vector. Various approach directions were simulated, since an lpc could impact from any direction. Varying approach directions provided a better sample space. Impact conditions are depicted in Figure 3.3 where θ measures the angle from the x axis to the direction of the incoming ECC in the xy plane and ϕ measures the angle from the θ direction to the ECC itself.

3-7
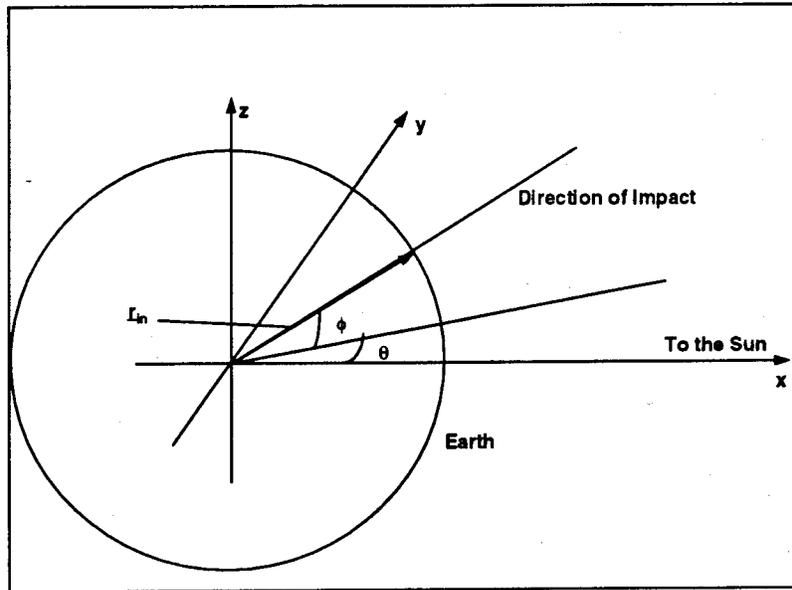
Figure 3.3. Conditions at impact (Final Conditions).

Given the conditions above, the final position of the ECC at impact in the xyz frame is:

$$x = -1 + \mu + R_e \cos(\phi)\cos(\theta) \qquad (3\text{-}19)$$

$$y = R_e \cos(\phi)\sin(\theta) \qquad (3\text{-}20)$$

$$z = R_e \sin(\phi) \qquad (3\text{-}21)$$

where R_e is the radius of the Earth in AUs. The position of the ECC at impact with respect to the Earth, r_{in}, is then:

$$r_{in} = \begin{bmatrix} R_e \cos(\phi)\cos(\theta) \\ R_e \cos(\phi)\sin(\theta) \\ R_e \sin(\phi) \end{bmatrix} \qquad (3\text{-}22)$$

and similarly, the velocity with respect to Earth is:

3-8

$$\mathbf{v}_{in} = \begin{bmatrix} v\cos(\phi)\cos(\theta) \\ v\cos(\phi)\sin(\theta) \\ v\sin(\phi) \end{bmatrix} \tag{3-23}$$

where $v = 60\text{km}/\text{sec} = 2.0\text{AU}/\text{TU}$ (1 TU = 58.13 days) is the "speed" of the ECC with respect to Earth.

Finally, applying Hamiltonian Dynamics to the restricted three-body equations of motion, the state at the final conditions may be found to be:

$$\mathbf{X} = \begin{bmatrix} q_1 \\ q_2 \\ q_3 \\ p_1 \\ p_2 \\ p_3 \end{bmatrix} = \begin{bmatrix} x \\ y \\ z \\ v\cos(\phi)\cos(\theta) - y \\ v\cos(\phi)\sin(\theta) + x \\ v\sin(\phi) \end{bmatrix} \tag{3-24}$$

3.3.2 Hamiltonian Dynamics and the Equations of Variation.. All of the dynamics contained in Subroutine Dynam are in fact Hamiltonian. The equations of motions, therefore, are represented as (13):

$$\dot{x} = p_1 + y \tag{3-25}$$

$$\dot{y} = p_2 - x \tag{3-26}$$

$$\dot{z} = p_3 \tag{3-27}$$

$$\ddot{x} = p_2 - \frac{(1-\mu)(x-\mu)}{r_1^3} - \frac{\mu(x+1-\mu)}{r_2^3} \tag{3-28}$$

3-9

$$\ddot{y} = p_1 - \frac{(1-\mu)y}{r_1^3} - \frac{\mu y}{r_2^3} \qquad (3\text{-}29)$$

$$\ddot{z} = -\frac{(1-\mu)z}{r_1^3} - \frac{\mu z}{r_2^3} \qquad (3\text{-}30)$$

Subroutine Dynam also calculates the "A" matrix which is defined as "the matrix of partial derivatives of the equations of motion with respect to the variables in the problem," or (14:115):

$$A(t) = \frac{\partial \mathbf{f}}{\partial \mathbf{X}} \qquad (3\text{-}31)$$

where $\mathbf{f}$ is a matrix of the system equations of motion, or:

$$\mathbf{f}(\mathbf{X},t) = \begin{bmatrix} \dot{x} \\ \dot{y} \\ \dot{z} \\ \ddot{x} \\ \ddot{y} \\ \ddot{z} \end{bmatrix} \qquad (3\text{-}32)$$

Finally, Subroutine Rhs calculates the equations of variation, which are the product of A and the state transition matrix, Φ ("the derivative of the state solution at time t with respect to the initial conditions at time t_o" [14:116]). The equations of variation and the equations of motion are then integrated in parallel to establish the ECC's trajectory.

3.3.3 Integrating the Trajectory.

Integrating the equations of variation and the equations of motions for a system such as the Restricted Three-Body problem, for

3-10

which no closed form solution exists, is known as a "Special Perturbations Differential Correction" (15:77). In order to integrate the ECC's trajectory, as indicated above, Dr. Wiesel's Haming numerical integration scheme, located in Subroutine Haming, has been used. "Haming is an ordinary differential equations integrator. It is a fourth order predictor-corrector algorithm which means that it carries along the last four values of the state vector, and extrapolates these values to obtain the next value (the prediction part) and then corrects the extrapolated value to fine a new value for the state vector" (13). Haming requires the initial state vector as well as the required timestep (A timestep, $h = 0.000001 TU = 0.0837 min$, has been used as the standard for all calculations). Two other variables, $nstp$ and nkp, control the number of times Haming is called and are related to the initial and final times for the trajectory as follows:

$$nstp = \frac{\left(t_f - t_o\right)}{h \cdot nskp} \tag{3-33}$$

The input files for Program Data contain the values for t_f, t_o, and $nskp$. These are used to calculate $nstp$, as above, and this value corresponds to the number of observations which will be generated.

3.3.4 Observation Simulation..

The final section of code in Program Data is responsible, in concert with Subroutine Obser, for generating simulated angles only observations for the ECC in question. In the "data loop" Obser is called $nstp$ times with each call producing one "perfect" observation (ob) of the position of the ECC.

Obser, as written, is capable of producing three types of angles-only obs: Earth-Based, ECO Detection Satellite 1 (EDS1), and ECO Detection Satellite 2 (EDS2). These data types are denoted numerically as 2, 3, and 4 respectively. This ob type is set in Program Data and for each call to Obser it is passed along so that the proper section of

code is referenced there. Let's discuss ob type 2 first since it is used for most of the calculations in this thesis.

Three primary results are calculated during each call to Obser. First, the inverse of the observation covariance matrix, Q^{-1}, is defined as:

$$Q^{-1} = \begin{bmatrix} Q_1^{-1} & 0 \\ 0 & Q_2^{-1} \end{bmatrix} \qquad (3\text{-}34)$$

where, assuming two independent angles only observations, the observation covariance matrix is:

$$Q = \begin{bmatrix} \sigma_1^2 & 0 \\ 0 & \sigma_2^2 \end{bmatrix} \qquad (3\text{-}35)$$

Here the σ^2 values represent the individual variances for each observed angle. Accuracies of 0.1 arcseconds (typical for most optical instruments) or 0.01 arcseconds (attainable by some) have been assumed. These values are represented, in radians, as the standard deviation, σ, for each observation, so that for an accuracy of 0.1 arcseconds:

$$Q_1^{-1} = Q_2^{-1} = \frac{1}{\sigma_1^2} = \frac{1}{(0.1\,\text{arcsec})^2} = \frac{1}{\left(4.85\cdot10^{-7}\text{radians}\right)^2} = 4.25\cdot10^{12} \approx 4.0\cdot10^{12} \quad (3\text{-}36)$$

and similarly for 0.01 arcsecond accuracy:

$$Q_1^{-1} = Q_2^{-1} = \frac{1}{\sigma_1^2} = \frac{1}{(0.01\,\text{arcsec})^2} = \frac{1}{\left(4.85\cdot10^{-8}\text{radians}\right)^2} = 4.25\cdot10^{14} \approx 4.0\cdot10^{14} \quad (3\text{-}37)$$

Second, the observation relation is defined and calculated. The observation relation is represented in the general case as (15:69):

$$z_i(t_i) = G(X(t_i), t_i) \qquad (3\text{-}38)$$

For our problem the angles to the ECC which would be actually measured (see Figure 3.4) would be stored in z, so that:

$$z = \begin{bmatrix} \alpha \\ \beta \end{bmatrix} \qquad (3\text{-}39)$$

However, since the observations are simulated, the equality in Equation (3-38) and the values produced by the G matrix (which contains the observed angles in terms of xyz coordinates) calculations are used to establish "perfect" obs. The G matrix then requires the state vector at the ob time in question; thus Haming is called following each call to Obser in order to provide it. Referencing Figure 3.4, the G matrix is defined as:

$$G = \begin{bmatrix} \arctan\left(\dfrac{y}{x+1-\mu}\right) \\ \arctan\left(\dfrac{z}{\sqrt{(x+1-\mu)^2 + y^2}}\right) \end{bmatrix} \qquad (3\text{-}40)$$

The calculations for types 3 and 4 observations differ only slightly from the Earth-based calculations. Figure 3.5 illustrates this. Comparing Figure 3.5 to Figure 3.4 one can see that by replacing $x+1-\mu$ and y, with $x+(1-\mu)\cos 60$ and $y+(1-\mu)\sin 60$, respectively, in the G and H matrices type 3 observations from the L5 position are generated. Similarly, a $-y+(1-\mu)\sin 60$ term generates type 4 obs from L4. Once "perfect" obs have been generated, errors must be introduced artificially. This is accomplished by adding randomly generated Gaussian noise which is produced in a call to function Randg.

3-13
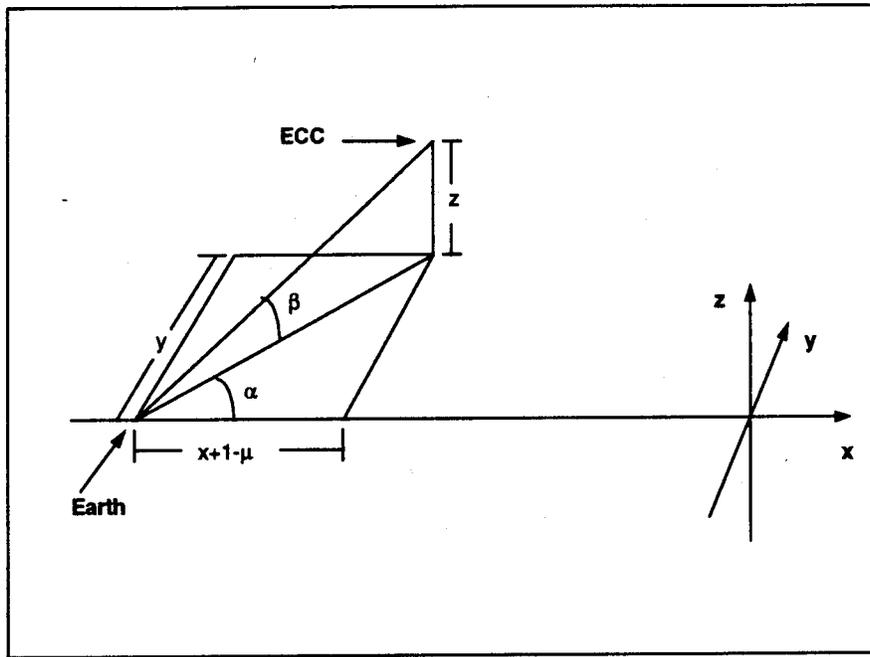
Figure 3.4. Earth-Based Observation Geometry.
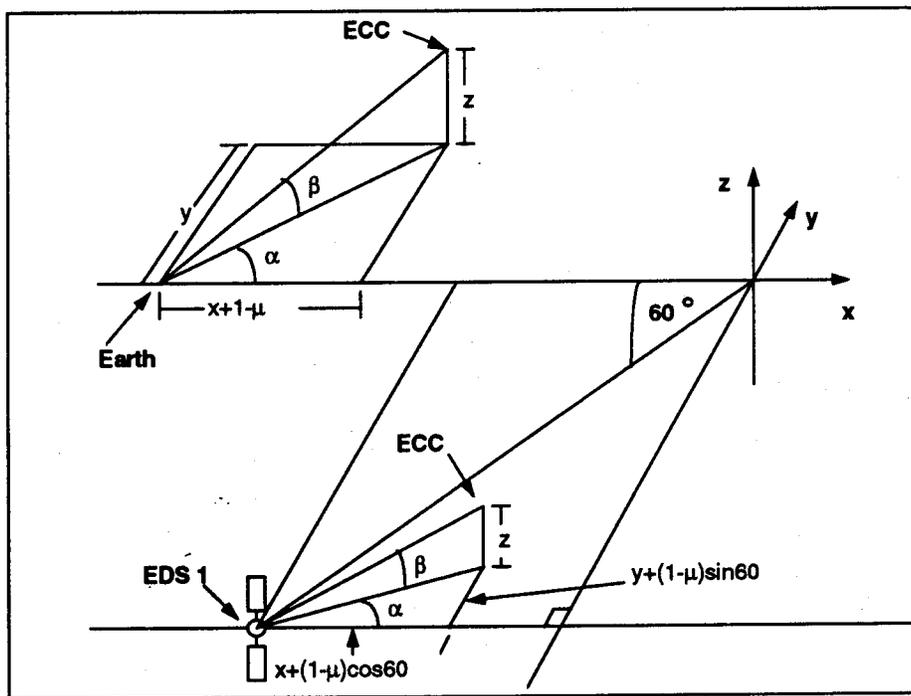
Figure 3.5. EDS 1 Observation Geometry.

3-14

Prior to being added to the "perfect" ob the random noise is divided by the square-root of the appropriate Q^{-1} value.

Finally, Obser calculates the **H** matrix, which will be discussed later since it is used by program Lstsq.

3.4 ECC Orbit Estimation

As alluded to, a Non-Linear Least Squares algorithm, program Lstsq, was used to estimate the state vector of each ECC using the simulated observations described above. This method is a well established one. It was first announced by Gauss in 1801 in its linear form but was quickly adapted to the non-linear case by Gauss himself (15:68).

Least Squares was chosen because although the Restricted Three-Body system under consideration here has no closed form solution, the dynamics predict the orbits of its bodies without error, in the absence of any other perturbing forces. What error exists comes from the inexactitude of the observations, and thus we have a "deterministic" system.

Least Squares produces an estimate of the state vector, given a reference trajectory, by minimizing the weighted squared sum of the observation residuals. These residuals are defined as the difference between the observed state, **z**, and the state predicted by the dynamics, **G**, or:

$$\mathbf{r}_i = \mathbf{z}_i - \mathbf{G}\left(\mathbf{X}_{ref}(t_i), t_i\right) \tag{3-41}$$

$\mathbf{X}_{ref}$ represents an initial "guess" of the state vector at the epoch time, or t_o in this case. This guess is the starting point for Least Squares estimation. The initial state vector, calculated by program Data, is used for my "guess". Once this is in hand Least Squares, for each supplied observation, propagates the state vector to the observation time and obtains the state transition matrix ("the gradient of the solution with respect to the initial

3-15

conditions" [15:33]) from subroutine Rhs. The residual vector is then calculated, along with an observation matrix,

$$T = \begin{bmatrix} T_1 \\ T_2 \\ \dots \\ T_N \end{bmatrix} = \begin{bmatrix} H_1 \Phi(t_1, t_o) \\ H_2 \Phi(t_2, t_o) \\ \dots \\ H_N \Phi(t_N, t_o) \end{bmatrix} \qquad (3\text{-}42)$$

where N is the number of observations taken and **H** "relates the error in the state to the error in the reference trajectory" (15:69). **H** is defined generally as (15:69):

$$H_i(t_i) = \frac{\partial G}{\partial X}\left(X_{ref}(t_i), t_i\right) \qquad (3\text{-}43)$$

and specifically here in subroutine Obser as:

$$H = \begin{bmatrix} \dfrac{\partial G_1}{\partial x} & \dfrac{\partial G_1}{\partial y} & \dfrac{\partial G_1}{\partial z} & \dfrac{\partial G_1}{\partial \dot{x}} & \dfrac{\partial G_1}{\partial \dot{y}} & \dfrac{\partial G_1}{\partial \dot{z}} \\ \dfrac{\partial G_2}{\partial x} & \dfrac{\partial G_2}{\partial y} & \dfrac{\partial G_2}{\partial z} & \dfrac{\partial G_2}{\partial \dot{x}} & \dfrac{\partial G_2}{\partial \dot{y}} & \dfrac{\partial G_2}{\partial \dot{z}} \end{bmatrix} \qquad (3\text{-}44)$$

where,

$$\frac{\partial G_1}{\partial x} = \frac{-y}{\left[(x+1-\mu)^2 \cdot \left[1 + \dfrac{y^2}{(x+1-\mu)^2}\right]\right]} \qquad (3\text{-}45)$$

3-16

$$\frac{\partial G_1}{\partial y} = \frac{1}{\left[(x+1-\mu)\cdot\left[1+\frac{y^2}{(x+1-\mu)^2}\right]\right]} \qquad (3\text{-}46)$$

$$\frac{\partial G_2}{\partial x} = \frac{-z(x+1-\mu)}{\left[\sqrt{(x+1-\mu)^2+y^2}\right]^3} \cdot \left[\frac{1}{1+\frac{z^2}{\left[(x+1-\mu)^2+y^2\right]}}\right] \qquad (3\text{-}47)$$

$$\frac{\partial G_2}{\partial y} = \frac{-yz}{\left[\sqrt{(x+1-\mu)^2+y^2}\right]^3} \cdot \left[\frac{1}{1+\frac{z^2}{\left[(x+1-\mu)^2+y^2\right]}}\right] \qquad (3\text{-}48)$$

$$\frac{\partial G_2}{\partial z} = \frac{1}{\sqrt{(x+1-\mu)^2+y^2}} \cdot \left[\frac{1}{1+\frac{z^2}{\left[(x+1-\mu)^2+y^2\right]}}\right] \qquad (3\text{-}49)$$

and

$$\frac{\partial G_1}{\partial z} = \frac{\partial G_1}{\partial \dot{x}} = \frac{\partial G_1}{\partial \dot{y}} = \frac{\partial G_1}{\partial \dot{z}} = \frac{\partial G_2}{\partial \dot{x}} = \frac{\partial G_2}{\partial \dot{y}} = \frac{\partial G_2}{\partial \dot{z}} = 0 \qquad (3\text{-}50)$$

When this is complete new terms are added to the matrices,

$$\sum_i \mathbf{T}_i^T \mathbf{Q}_i^{-1} \mathbf{T}_i \qquad (3\text{-}51)$$

and

$$\sum_i \mathbf{T}_i^T \mathbf{Q}_i^{-1} \mathbf{r}_i \qquad (3\text{-}52)$$

3-17

which are used to calculate the covariance of the correction,

$$P(t_o) = \left(\sum_i \mathbf{T}_i^T \mathbf{Q}_i^{-1} \mathbf{T}_i \right)^{-1} \tag{3-53}$$

and the state correction vector at epoch:

$$\delta \mathbf{X}(t_o) = \mathbf{P}(t_o) \cdot \sum_i \mathbf{T}_i^T \mathbf{Q}_i^{-1} \mathbf{r}_i \tag{3-54}$$

Finally, the reference trajectory is corrected,

$$\mathbf{X}_{ref+1}(t_o) = \mathbf{X}_{ref}(t_o) + \delta \mathbf{X}(t_o) \tag{3-55}$$

and if convergence has been achieved then we have an estimate, $\mathbf{X}_{ref}$, of the state with covariance $\mathbf{P}_x$ (15:72).

With an estimated state vector and covariance calculated the residuals of the Least Squares corrections were checked to be within an acceptable range of σ. If this was indeed the case then the correction was deemed valid.

3.5. Impact Prediction

Finally we arrive at calculating the information which is the goal of this thesis. These calculations were done as a part of program Lstsq since all the necessary information is contained therein.

The first step is to numerically integrate the estimated state vector and Φ to the impact time. The necessary number of calls to Haming are first calculated by making use of the state epoch time, impact time, and timestep information. Then the state vector is integrated to impact time and Φ extracted from it.

Second, the state covariance matrix is propagated to the impact time using subroutine Phpph. Phpph makes use of the relation (15:34),

$$\mathbf{P}_x(t_f) = \Phi(t_f, t_o)\mathbf{P}_x(t_o)\Phi^T(t_f, t_o) \qquad (3\text{-}56)$$

which holds only for deterministic systems where the covariance has not grown too large. This is because it involves Φ, "which is a linearization of the underlying nonlinear dynamics" (15:35). If the covariance, or error ellipsoid, grows too large it leaves the linear regime of the dynamics (15:35). $\mathbf{P}_x(t_f)$ contains all the information needed to calculate the appropriate error axis with which we are concerned.

$\mathbf{P}_x(t_f)$ is a 6x6 matrix, but the "space" part of it, or the upper left 3x3, is the only part of interest here. It is in this submatrix, denoted $\mathbf{P}_r$, that the information pertaining to the "impact dispersion on the Earth's surface" is contained. At the moment of impact the velocity (now zero) and the local vertical position (the local Earth radius) information are
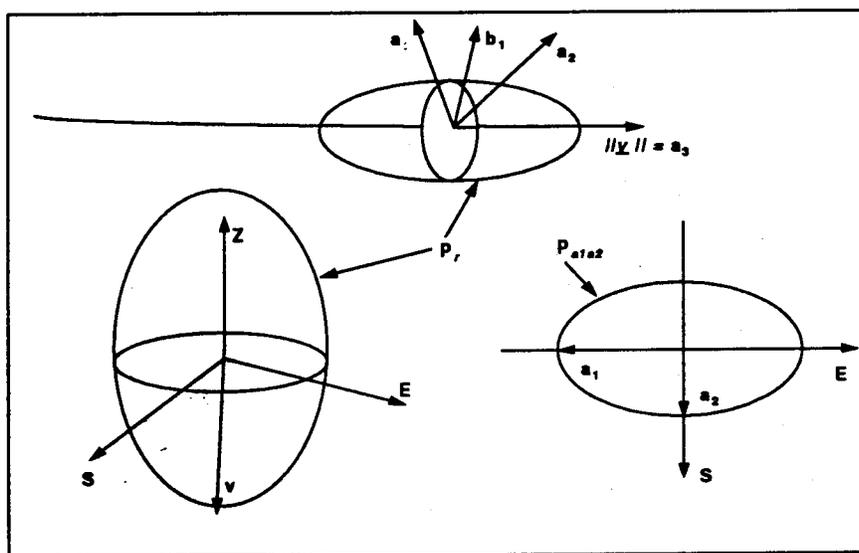
Figure 3.6 Position Error Ellipsoid in the Topocentric Frame (15:46).

3-19

perfectly known. The local vertical information can be discarded by transforming to a local topocentric frame of reference, **SEZ**. Let's begin by defining the $\mathbf{a_3}$ vector as the normal of the velocity vector, $\|\mathbf{v}\|$, where,

$$\mathbf{v} = \begin{bmatrix} \dot{x} \\ \dot{y} \\ \dot{z} \end{bmatrix} \tag{3-57}$$

Then, defining a vector perpendicular to $\mathbf{a_3}$ as $\mathbf{b_1} - (\mathbf{b_1} \cdot \mathbf{a_3})\mathbf{a_3}$, where,

$$\mathbf{b_1} = \begin{bmatrix} 1 \\ 0 \\ 0 \end{bmatrix} \tag{3-58}$$

$\mathbf{a_1}$ is found to be,

$$\mathbf{a_1} = \frac{\mathbf{b_1} - (\mathbf{b_1} \cdot \mathbf{a_3})\mathbf{a_3}}{\|\mathbf{b_1} - (\mathbf{b_1} \cdot \mathbf{a_3})\mathbf{a_3}\|} \tag{3-59}$$

and

$$\mathbf{a_2} = \mathbf{a_1} \times \mathbf{a_3} \tag{3-60}$$

This allows us to define the **XYZ** to **SEZ** rotation matrix,

$$\mathbf{R} = \begin{bmatrix} \mathbf{a_1} & \mathbf{a_2} & \mathbf{a_3} \end{bmatrix} \tag{3-61}$$

The "space" part of the state covariance matrix in the **SEZ** coordinate system is then,

$$\mathbf{P}_{ra} = \mathbf{R}\mathbf{P}_r\mathbf{R}^T \tag{3-62}$$

3-20

The upper left 2x2 submatrix of this 3x3 matrix is denoted $\mathbf{P}_{a1a2}$ and the axis lengths a_1 and a_2 are the square roots of the eigenvalues of this matrix. It is these two axis lengths which indicate "the impact dispersion on the Earth's surface." These values could be used to calculate the Circular Error Probable (CEP) for the ECCs. However only the axis lengths themselves are presented because "for very oblique trajectories . . . " the CEP "may be a vast underestimate of the actual error behavior" (15:47). This is because it reduces the a_1 and a_2 "axes to the radius of the circle with the same area" and "corrects the one sigma error ellipsoid to the 50 % probability ellipsoid" (15:47). Finally, the time uncertainty of impact is the square root of the row 3, column 3 entry in $\mathbf{P}_{ra}$, since as a 1x1 matrix it is its own eigenvalue.

IV. Results and Analysis

The worst case scenario for an ECC on a collision course with Earth (short of our never detecting it) is that we detect the ECC with only a few weeks notice. In such a situation we would have little time to determine whether or not the ECC is a threat and, if so, to react. The next section presents such a scenario.

4.1 Trajectory 1: The "No Warning Category."

Assuming we have detected an ECC with exactly three weeks notice and have determined its orbit well enough to know that it may be a threat, we would most likely use every means at our disposal to track it. Therefore this first scenario includes a relatively small ob interval that is a multiple of the programmed time-step. The conditions read into program Data were:

- Time of Detection: 0000, 22 November 1994
- Time of Impact: 0000, 13 December 1994
- Impact Direction: $\phi = 45^0$, $\theta = 90^0$
- Observation Interval: 8.371126 minutes

Integration of these initial conditions produced the trajectory in Figure 4.1 and Figure 4.2.

The first approach to estimating the impact point for this trajectory was to attempt a Lstsq correction on each day beginning on the detection day, 21 days from impact, and ending on the final day; each correction included the current day's obs, plus all other obs since detection, a "cumulative" approach. The accuracy of the obs was set to 0.1 arcseconds. Looking at Figure 4.3, one can see that the cumulative approach resulted in sporadic results with no Lstsq estimates after day 18. This lack of estimates was due to Lstsq's inability to accept all of the observations (Lstsq failed to read any more obs after day 18). The sporadic results were also probably due to an excessive number of observations (3,612 to be exact) over the 3 week period. Consequently, the second

4-1
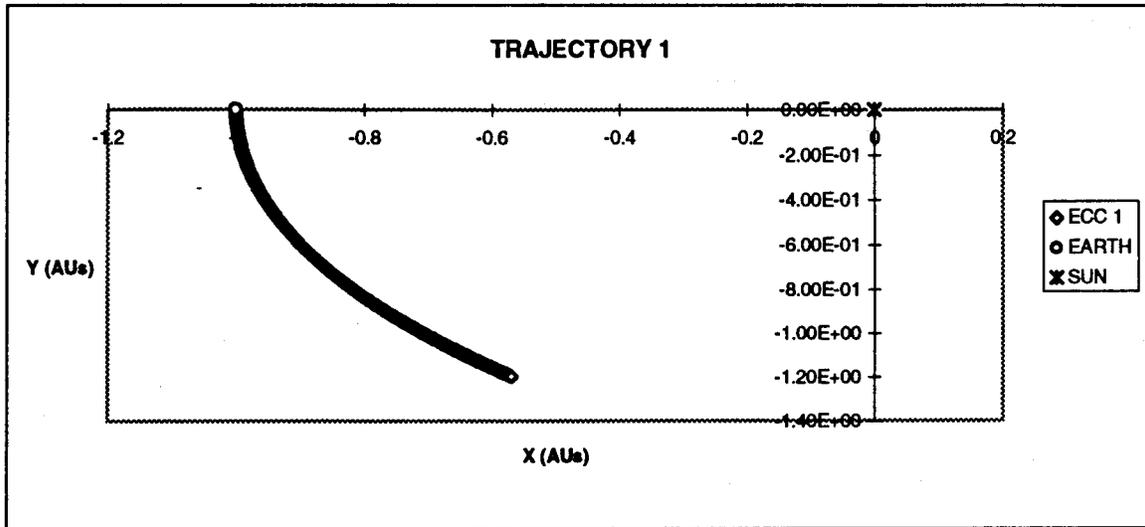
TRAJECTORY 1

Figure 4.1 Trajectory 1: Simulated Detection 3 Weeks Before Earth Impact.
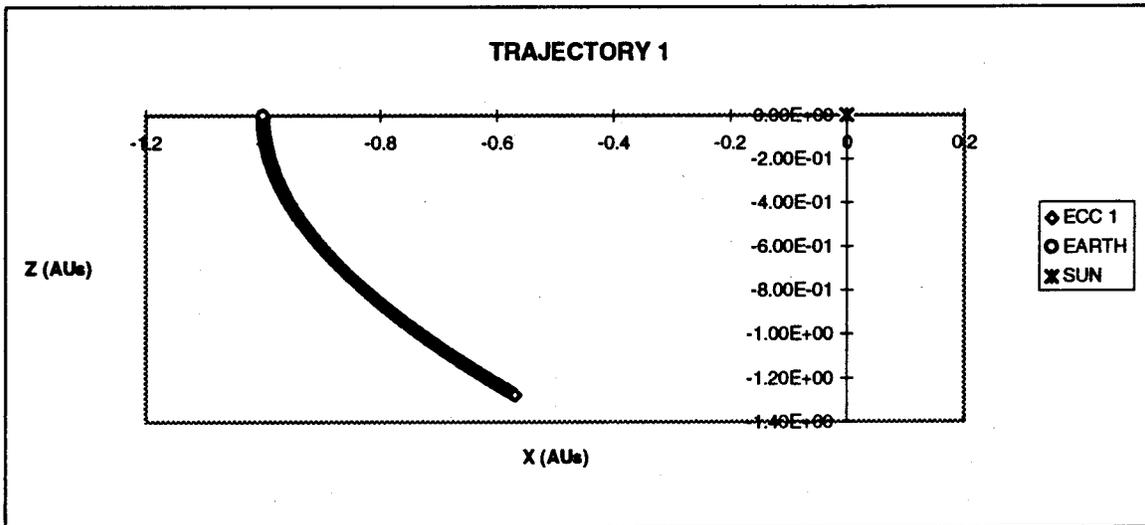
TRAJECTORY 1

Figure 4.2. Trajectory 1: Simulated Detection 3 Weeks Before Earth Impact.

run used only the last five days' worth of obs for each Lstsq estimate. This provided somewhat more consistent corrections and a correction for each of the 21 days. Most importantly, only four Lstsq estimates produced an impact prediction whose error was within one Earth radius, and all of these estimates were produced using the "5 day obspan" approach. The best estimate occurred 12 days following detection, which would

4-2
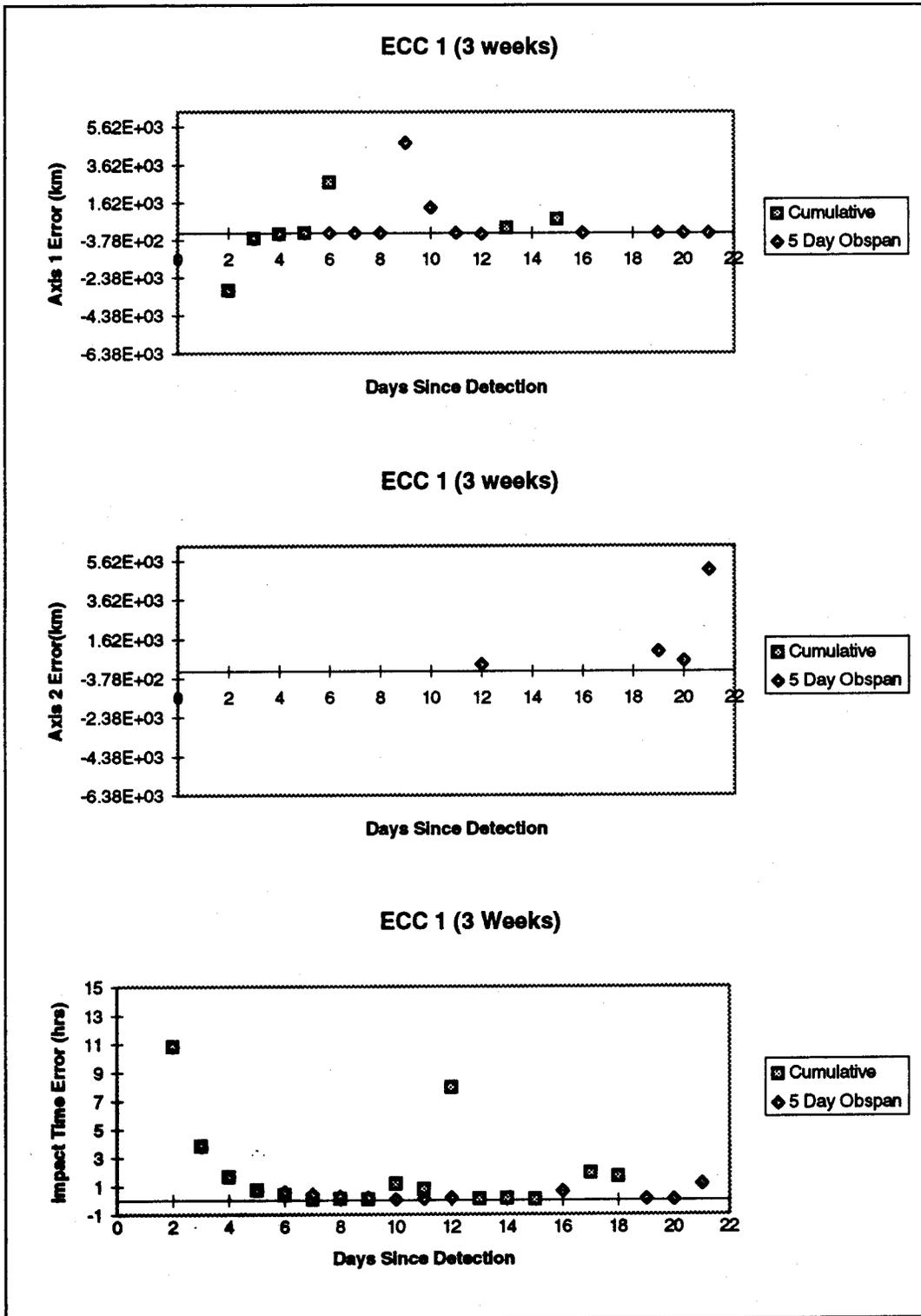
Figure 4.3. Trajectory 1: Cumulative vs 5 Day Obspan with 0.1 arcsec Accuracy.

ECC 1 (3 Weeks)

ECC 1 (3 Weeks)

ECC 1 (3 Weeks)
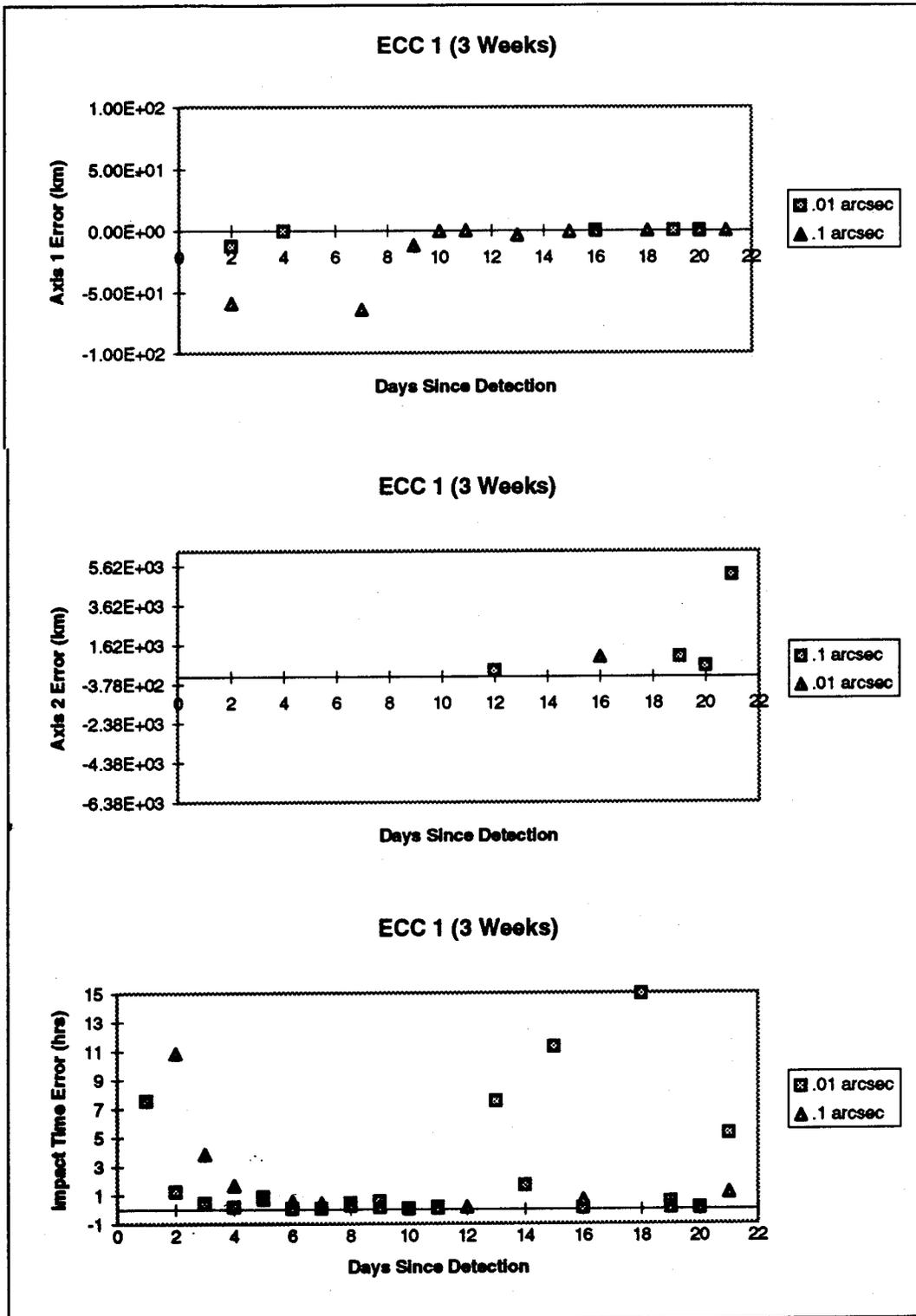
Figure 4.4 Trajectory 1. 5 Day Obspans, 0.1 vs 0.01 arcsec

offer only 9 days warning prior to impact (the term "warning" to indicates the number of days before impact that both error axes, or the impact footprint, were/was within an Earth radius. This is not to say that the impact point is known exactly within these axes. The error axes extend from the estimated state vector which may not coincide exactly with the true state vector). This disappointing result, which would offer little reaction time, led to another set of observations where the accuracy was increased to 0.01 arcseconds.

Strangely enough the 0.01 arcsec data offered little or no improvement over the 0.1 arcsec data. In fact they produced only one impact prediction with both error axes within an Earth radius (see Figure 4.4.). Notice that the impact time predictions are much better behaved than the axes predictions and that they are accurate enough that contingency planning could certainly be taken based on that knowledge alone. Also, axis 1 for this trajectory is much better known than axis 2, so that the error axes form a narrow "corridor". The best prediction, at nine days out, forms a corridor that is 60 km by 320 km.

4.2 The "Immediate Threat Category".

The ineffectiveness in predicting the impact for the preceding case is likely due to the ECC's apparent straight-in approach when only three weeks away. Consequently, the remaining trajectories assume detection at three months out. Trajectory 1 was integrated over this time frame, followed by numerous other trajectories . All of the remaining trajectories lie entirely in the xy plane, so that $\phi = 0.0$. θ was varied to distribute the impact directions somewhat evenly among the possibilities within 360^0. Therefore the conditions fed into program Data were:

- Time of Detection: 0000, 13 September 1994
- Time of Impact: 0000, 13 December 1994

4-5
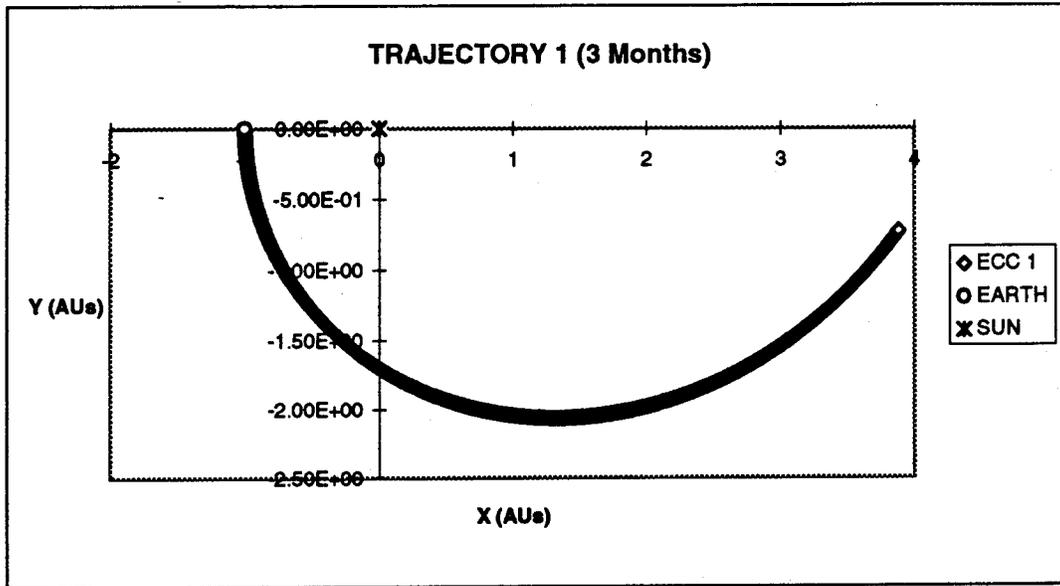
Figure 4.5. Trajectory 1: Simulated Detection 3 Months Before Earth Impact.
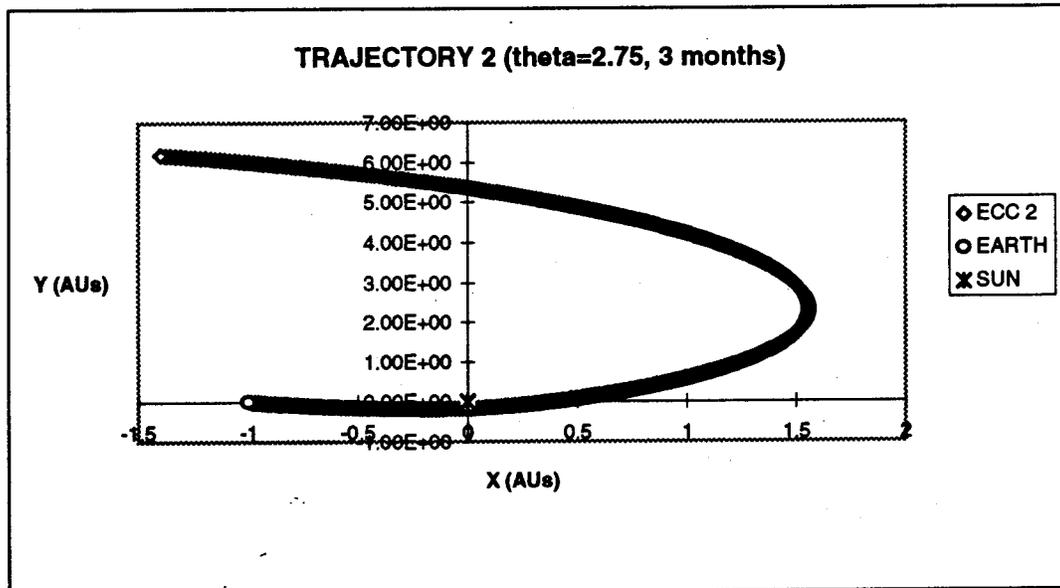
Figure 4.6. Trajectory 2: Simulated Detection 3 Months Prior to Earth Impact.

4-6
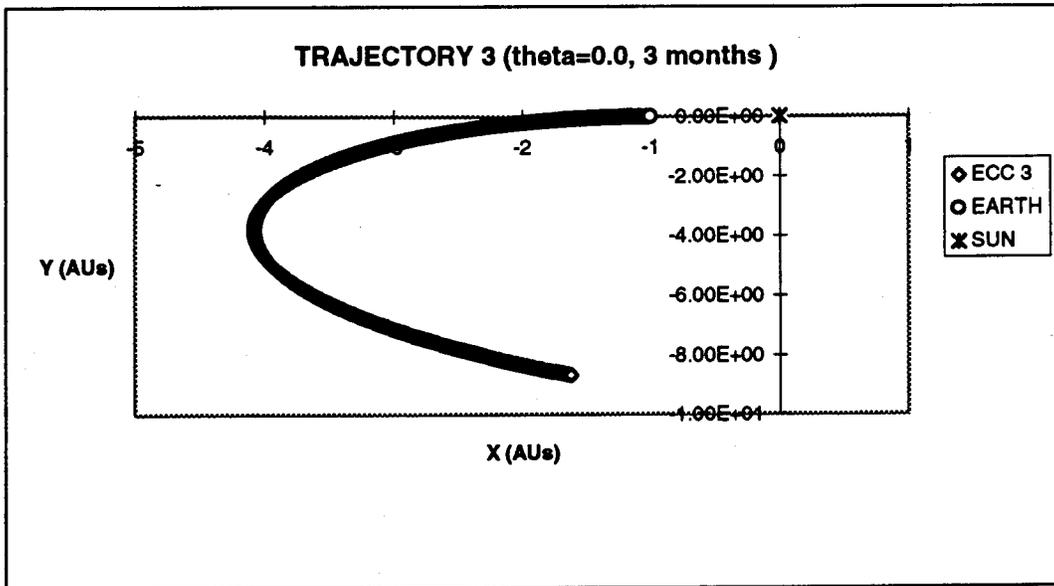
Figure 4.7. Trajectory 3: Simulated Detection 3 Months Prior to Earth Impact.
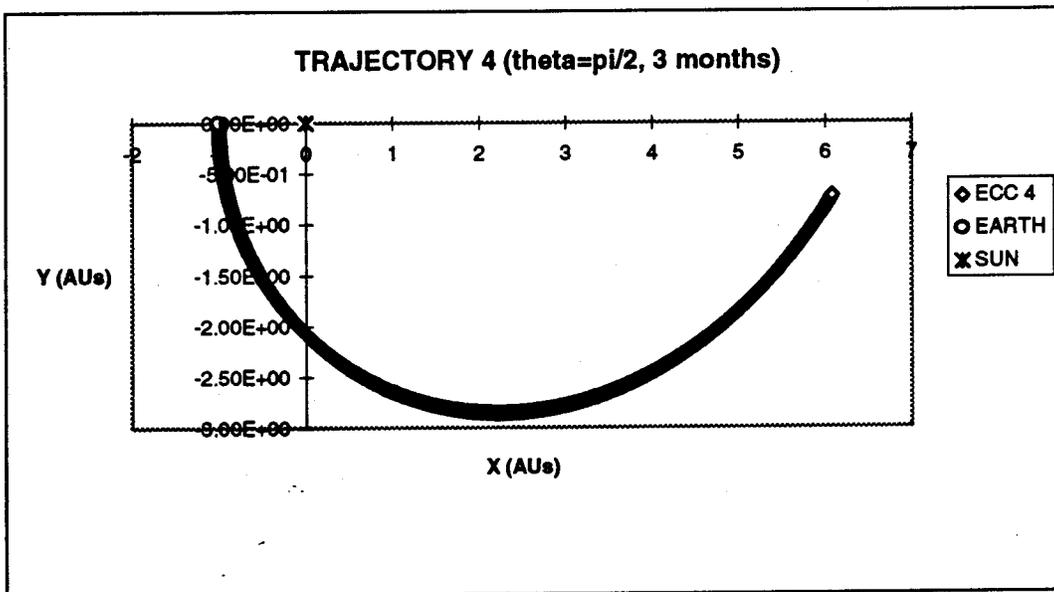
Figure 4.8. Trajectory 4: Simulated Detection 3 Months Prior to Earth Impact.

TRAJECTORY 5 (theta=pi/4, 3 months)

Y (AUs)

X (AUs)

◇ ECC 5
○ EARTH
✖ SUN
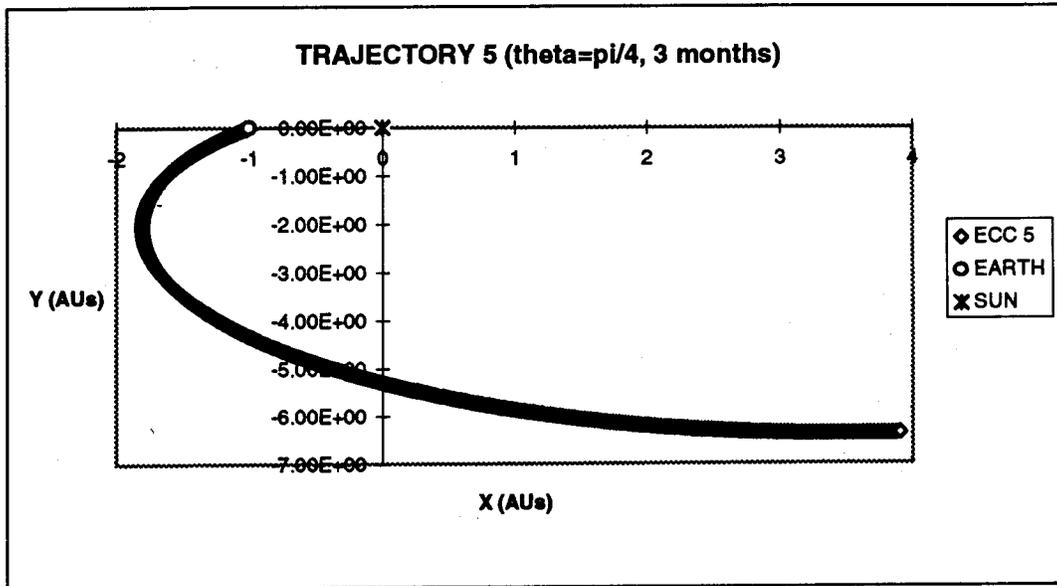
Figure 4.9. Trajectory 5: Simulated Detection 3 Months Prior to Earth Impact.

TRAJECTORY 6 (theta=3pi/4, 3 months)

Y (AUs)

X (AUs)

◇ ECC 6
○ EARTH
✖ SUN
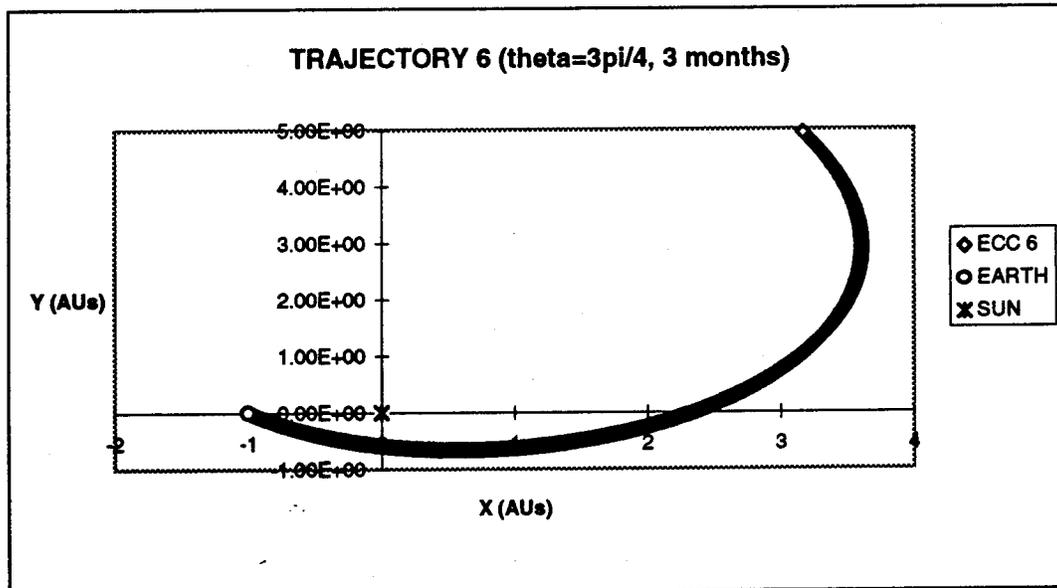
Figure 4.10. Trajectory 6: Simulated Detection 3 Months Prior to Earth Impact.
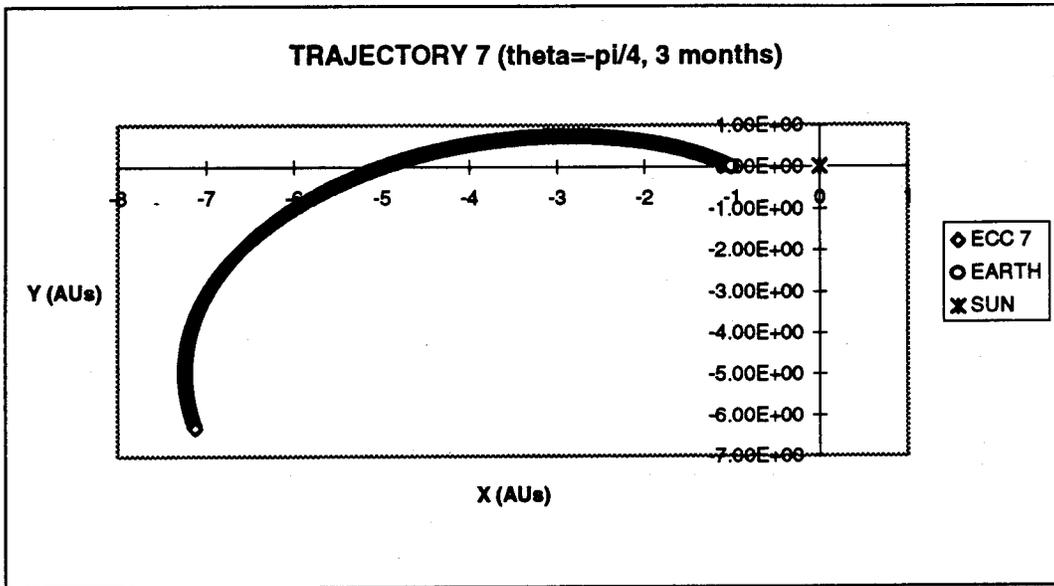
Figure 4.11. Trajectory 7: Simulated Detection 3 Months Prior to Earth Impact.
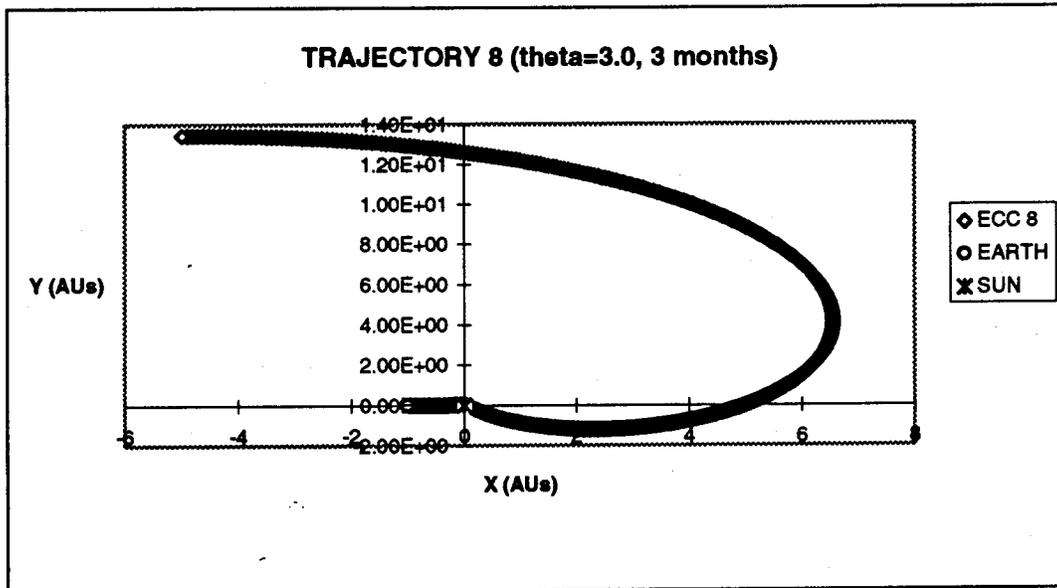
Figure 4.12. Trajectory 8: Simulated Detection 3 Months Prior to Earth Impact.

4-9
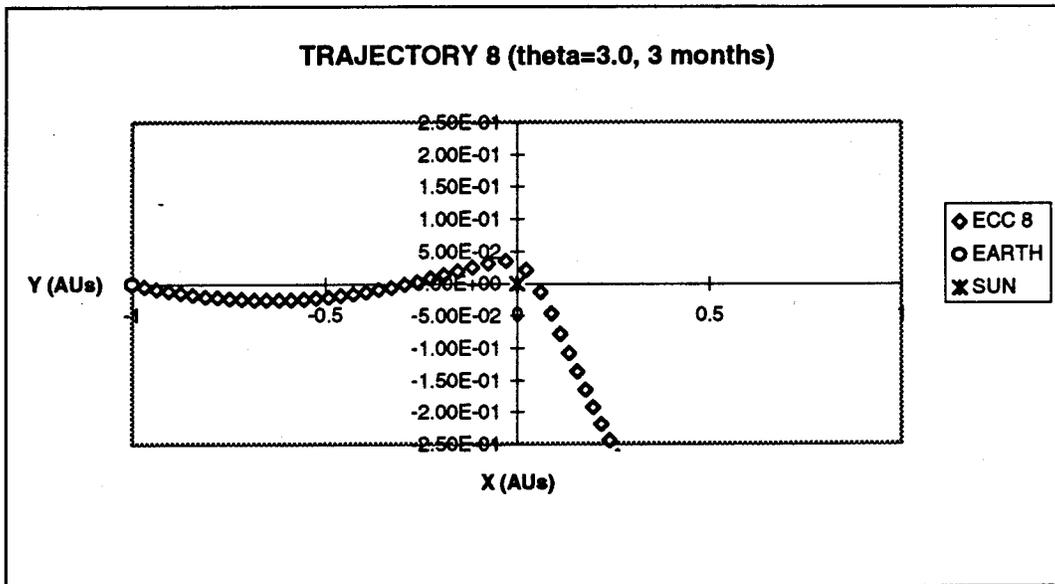
Figure 4.13. Trajectory 8: Close Approach to the Sun.

- Impact Directions: $\phi = 0.0$, $\theta = 2.75$, 0.0, $\pi/2$, $\pi/4$, $3\pi/4$, $-\pi/4$, 3.0 (in radians) for trajectories 2, 3, 4, 5, 6, 7, and 8, respectively.

- Observation Intervals: varied with a baseline of 262.605208652 minutes.

This thesis contains least squares estimates on trajectories 1-4 only. The remaining trajectories demonstrate further samples of orbits. Notice that several of them spend a great deal of time in the vicinity of the Sun during final approach to Earth. This would obviously create great operational difficulties for optical telescopes trying to obtain observations from Earth due to opposition from the Sun. For this reason these trajectories provide a compelling argument for placing EDSs at some location far from Earth.

4.2.1 A Baseline Comparison. As indicated, Lstsq estimates for the first four trajectories used the baseline obs interval of approximately 4.38 hours. Estimates were made, first with ob spans of five days (as in the second run for trajectory 1 with 3 weeks warning) but the results were better using the cumulative approach in this case (This

4-10

ECCs 1,2,3, and 4. (3 months)

ECCs 1,2,3, and 4 (3 months)

ECCs 1,2,3, and 4 (3 months)
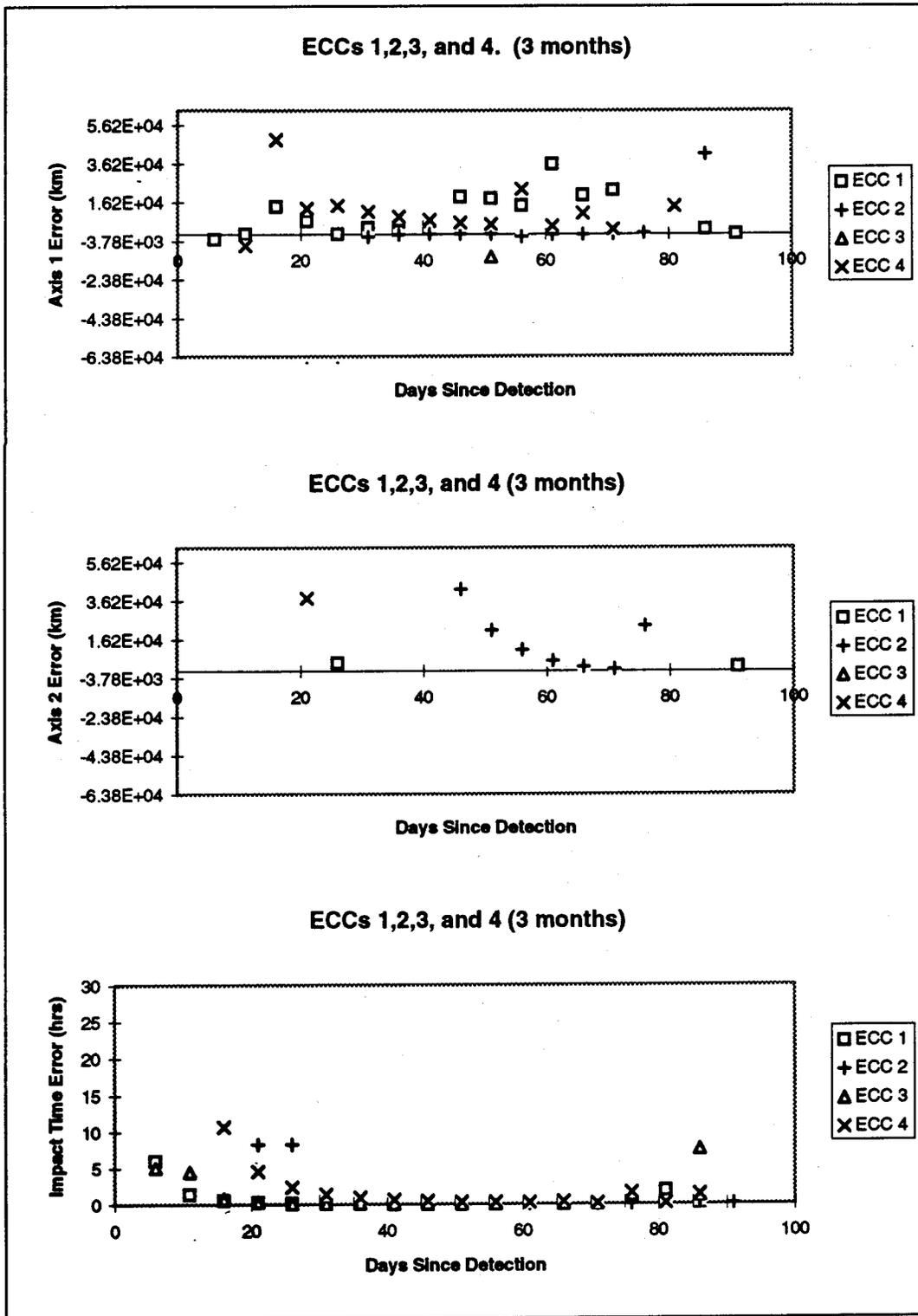
Figure 4.14. Trajectories 1,2,3, and 4: Baseline Errors Within 10 Earth Radii..

Trajectories 1,2,3, and 4. (3 months)

Axis 1 Error (km)

5.62E+03
3.62E+03
1.62E+03
-3.78E+02
-2.38E+03
-4.38E+03
-6.38E+03

20   40   60   80   100

Days Since Detection

□ ECC 1
+ ECC 2
△ ECC 3
✕ ECC 4

ECCs 1,2,3, and 4 (3 months)

Axis 2 Error (km)

5.62E+03
3.62E+03
1.62E+03
-3.78E+02
-2.38E+03
-4.38E+03
-6.38E+03

20   40   60   80   100

Days Since Detection

□ ECC 1
+ ECC 2
△ ECC 3
✕ ECC 4

ECCs 1,2,3, and 4 (3 months)

Impact Time Error (hrs)

2
1.5
1
0.5
0

0   20   40   60   80   100

Days Since Detection

□ ECC 1
+ ECC 2
△ ECC 3
✕ ECC 4

Figure 4.15. Trajectories 1,2,3, and 4: Baseline Errors Within 1 Earth Radius.

data is in the Appendix). "Expanding memory estimation," "the strategy of keeping all of the data ever taken in the estimate," can sometimes lead to the state covariance tending towards zero (15:89). This effect will occur "even if we used a perfect state model in a perfectly deterministic situation" (15:88). This fact likely explains the inferior results obtained for the cumulative approach used on the three week runs for trajectory 1. The tactic of "finite memory estimation," which is the method of using only "current" data for a "current" estimate, serves as a means of combating the zero covariance tendency (15:89). This is likely the reason that trajectory 1 allowed better results with the five day obspan approach. However, as indicated, the reverse of these results seemed to occur for the three month runs. This is likely a result of the much greater ob interval used in the three month case (8 minutes verses 263 minutes). In least squares estimation there is a trade off of "data quantity and quality against data time interval" (15:89). With this in mind, let's discuss the baseline comparison of the first four trajectories using the 263 minute ob interval and a cumulative approach with corrections every five days of the 91 day trajectories.

One can see in Figure 4.14 that only three of the four trajectories resulted in a correction with both error axes within 10 Earth radii. Once again, however, the axis one errors were much smaller, forming an error corridor. However, this time the error corridors are much wider and longer, so that only two trajectories, ECCs 1 and 2, resulted in a one sigma impact footprint that was within one Earth radius (see Figure 4.15). The time errors, as before, are much better behaved and relatively small. Comparing these results with those for trajectory 1 at three weeks out suggests that increasing the number of observations can result in a much better estimate. Recall the estimate in that run that was 60 by 320 km, and compare it to the best estimates here of 83 by 4000 km 65 days before impact for ECC 1 and 75 by 780 km 20 days out for ECC 2. ECC 2 also had predictions within one Earth radius as early as 30 days out. The one bright note here is

4-13

that for at least two of the four trajectories we could predict an Earth impact perhaps early enough to avert it (depending on the intercept and deflection technologies).

One more important result to note from the baseline corrections is that these corrections, which generally improve as the ECC approaches Earth, display increasing axis one and time errors past a point which is about 10 to 30 days prior to impact. This can be seen in the Impact Time Error data in Figure 4.15 and in Figure 4.16 for axis one. This same phenomenon occurs for axis two, albeit earlier, perhaps 30 to 50 days before impact.
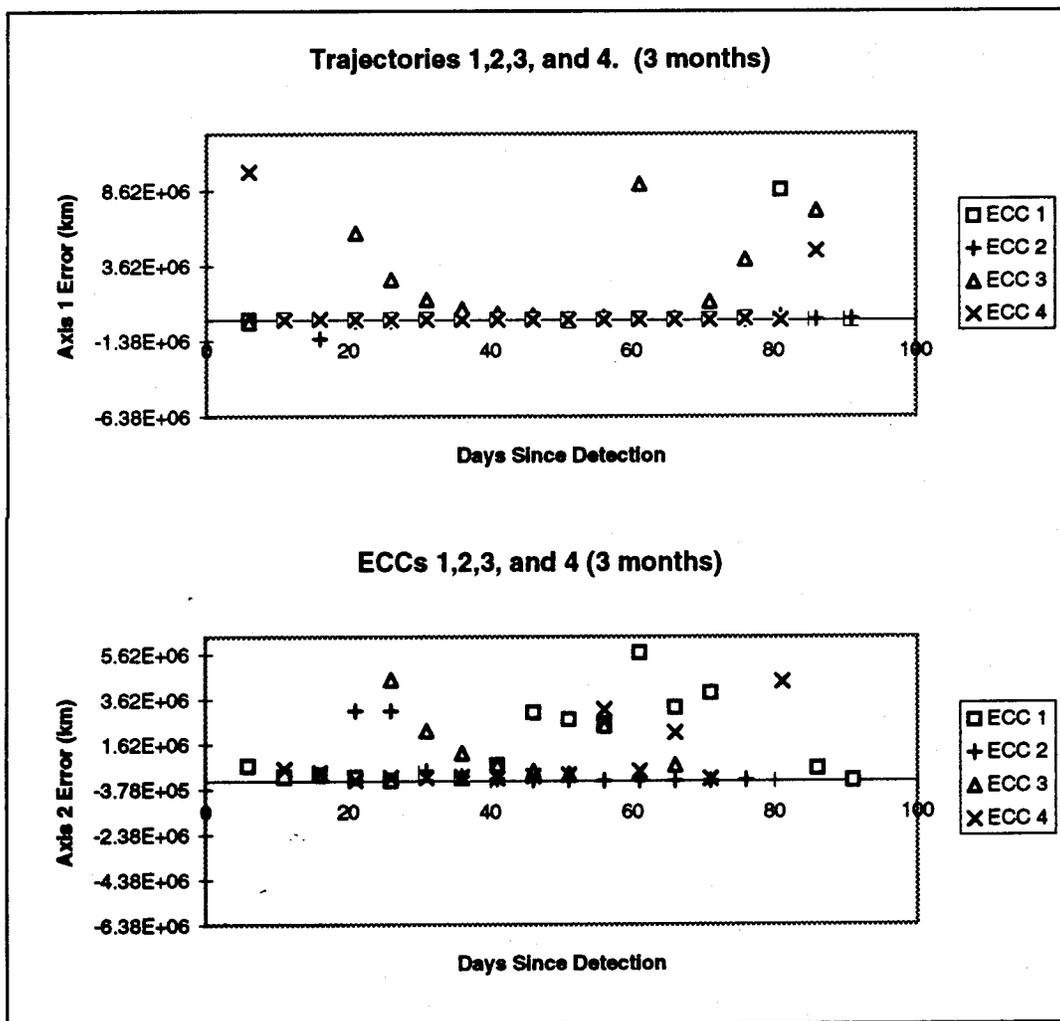
Figure 4.16. Trajectories 1,2,3, and 4: Baseline Error Increase at Earth Approach.

4-14

4.2.2 Increasing the Number of Observations. Considering the much more accurate estimate obtained for ECC 1 on the 3 week run, albeit "late in the game," the number of observations were increased by a factor of 10 over the three month period for trajectory 2 to see what the results would be. No real improvement was noted(see Figure 4.17). Both error axes were within one Earth radius 20 days later (10 days out rather than 30). This is perhaps a result of too much data for Lstsq to be successful even though only 5 days' worth of obs were used for each estimate. This is opposite from the three week run results.

4.2.3 Increasing the Accuracy. Although increasing the accuracy from 0.1 arcsec to 0.01 arcsec seemed to offer little or no improvement in the estimates for trajectory 1 three weeks out, it was worth testing over a three month period. This is because the lack of improvement for ECC 1 three weeks out was probably due to the unfortunate geometry of having the ECC so close and appearing to come straight in. The results from obs using 0.01 arcsec accuracy are seen in Figure 4.18. There was some general improvement over the 0.1 arcsec accuracy as you can see for these charts showing errors within 1,000 Earth radii. However, neither the 0.1 arcsec run nor the 0.01 arcsec run resulted in a single estimate in which both error axes were within one Earth radius.

4.2.4 Simulated Remote Tracking. As stated earlier, it's likely that the less than encouraging results obtained to this point were caused by the geometry when taking observations from the impact point (Earth). To test this, trajectory 9, which "impacted" at some point away from but in the vicinity of Earth, was created. This trajectory is depicted in Figure 4.19. Lstsq estimates for this trajectory were made using the baseline approach of 499 obs over three months, with cumulative 0.1 arcsec accuracy runs. The results are found in Figure 4.20. As one can see they are profoundly different than any of the results

4-15

for the four Earth impacting ECCs. Both error axes are much better behaved with each of them reaching values below one Earth radius by day 51 or 40 days prior to "impact". From there the estimate continues to improve right up until day 91 with the error reaching dimensions of 0 by 80 km both 5 days out and on the day of "impact".

4.2.5 ECO Detection Satellite Observations.

4.2.5.1 Tracking with One EDS. Very much encouraged by the results of the previous section, EDS obs were used to estimate one of the original four Earth impacting trajectories. These obs were first simulated from L5, located in the Earth's orbit at -60 degrees from the x axis in the restricted three-body frame. The position of both the EDS satellites and the trajectories of ECCs 1 and 3 are displayed in Figure 4.21. The EDS 1 observations were simulated for ECC 3 under the baseline approach and the results are depicted in Figure 4.22. These results are somewhat disappointing since Lstsq failed to converge to a solution past the day 66 estimate. On the other hand, this run included the only estimate so far for ECC 3 in which both axes could be predicted within one Earth radius. This definitely confirms the effectiveness of obtaining obs from a remote location, especially considering that the Earth-based obs were 10 times as accurate than those from the EDS.

4.2.5.2 Tracking with EDS and Earth Obs Combined. Still not achieving results as good as those for trajectory 9, it was theorized that trajectory 3 was simply a more difficult orbit to predict. This is supported by a comparison to the other three trajectories in the baseline results. Also, looking at Figure 4.21, one can see that ECC 3 appears to spend most of its final month and a half on a relatively straight in
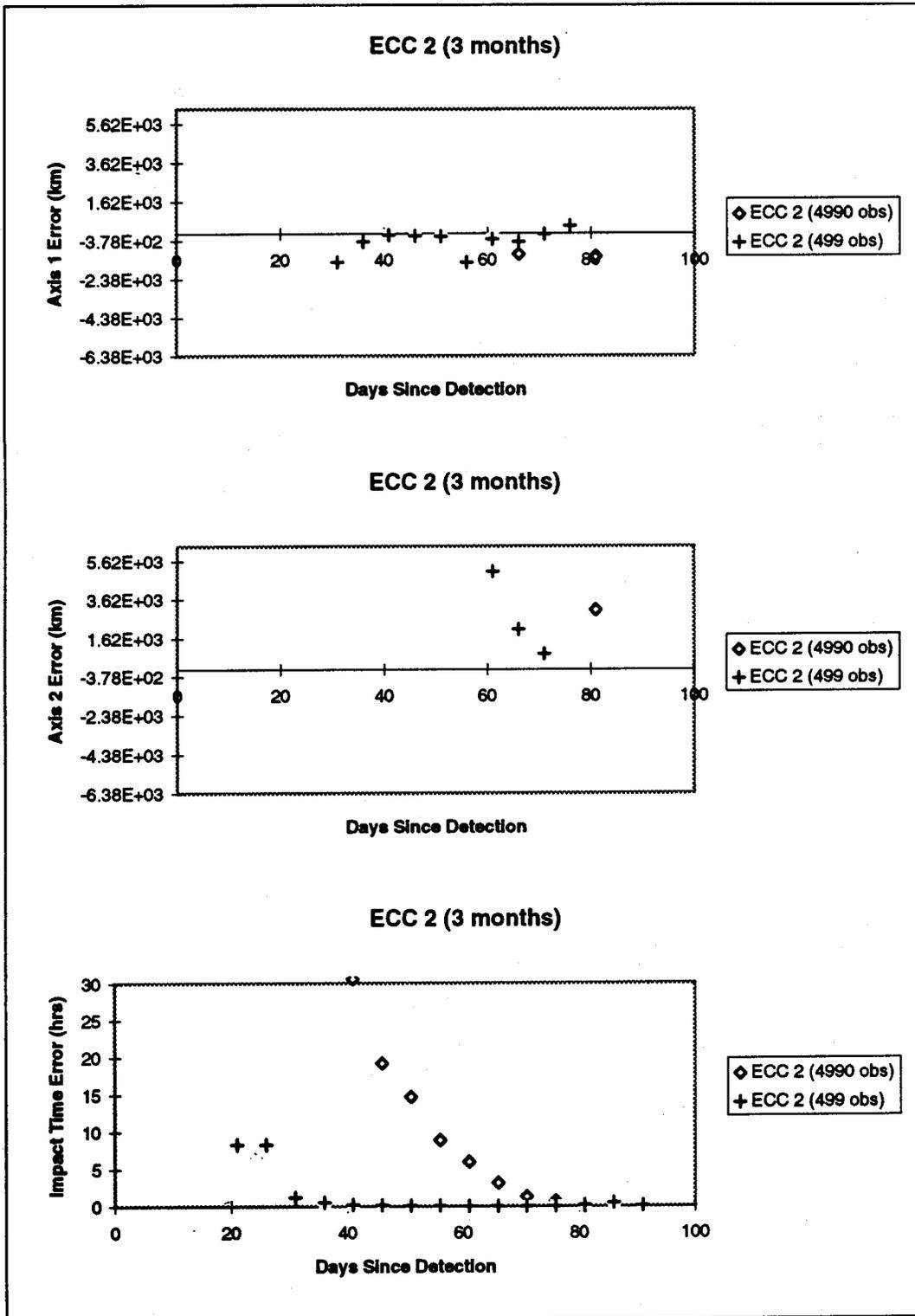
Figure 4.17. Trajectory 2: Baseline vs 10 Times as Many Obs.
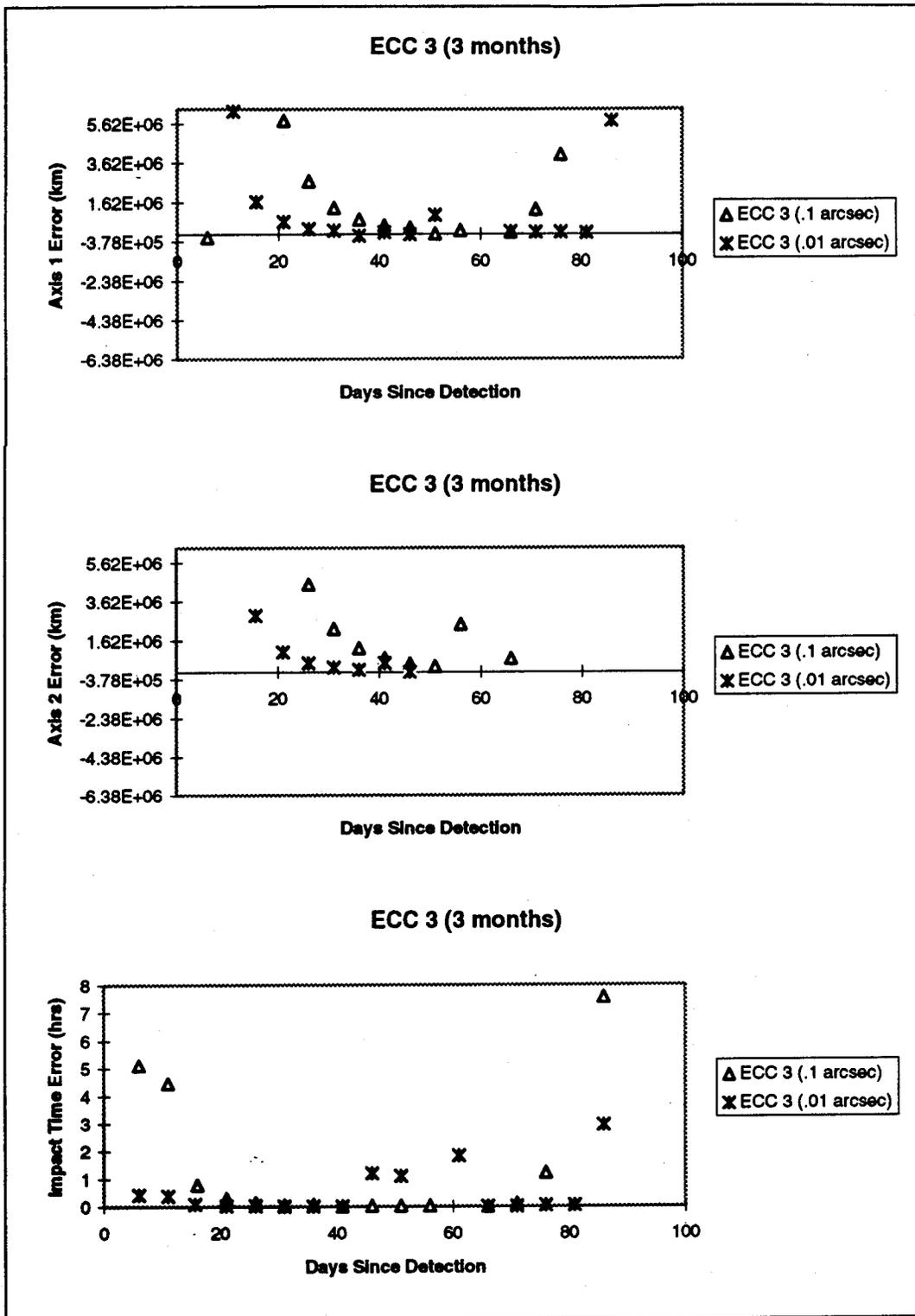
Figure 4.18. Trajectory 3: Baseline vs 0.01 arcsec Accuracy.

TRAJECTORY 9 (x=-1.5,y=-.5,ydot=60km/sec)

Y (AUs)

X (AUs)

◆ ECC 9
○ EARTH
✗ SUN
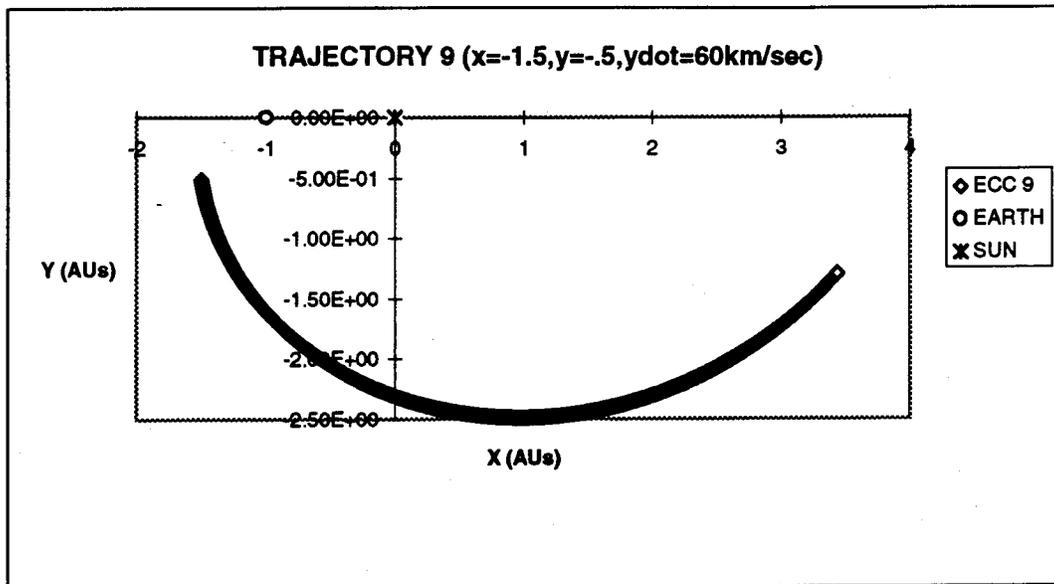
Figure 4.19. Trajectory 9: Simulated Detection 3 Months Prior to Reaching the Position and Velocity Indicated Above.

trajectory with respect to the Earth and perhaps even EDS 1. Consequently, EDS 2 obs were combined with both Earth and EDS 1 obs. All three accuracies were set to 0.1 arcsec for the first run. Initially, the observation interval was left the same as the baseline approach which resulted in 499 obs from each source. When these results did not come out as hoped, the obs interval was tripled so that we were again left with 499 obs total for the three month period spread equally among EDS 1, 2, and Earth obs. These were fed into Lstsq just as with the baseline estimates. The results for ECC 3 are in Figure 4.23. Once again, the differential corrections failed to converge past day 66 and not all of the estimates were an improvement, on a point by point basis, over the EDS 1 only run. However, the estimates which are better seem to come closer to the detection time so that the day on which both error axes come within one Earth radius is 15 days sooner; this occurs 55 days before impact. Also, the smallest axis two error is an order of magnitude less. It was found that since the axis errors seem to be sporadic, the time errors, which are better behaved, are a good indicator for comparison. One can see in Figure 4.23 that they

4-19

ECC 9 (3 months)

ECC 9 (3 months)

ECC 9 (3 months)
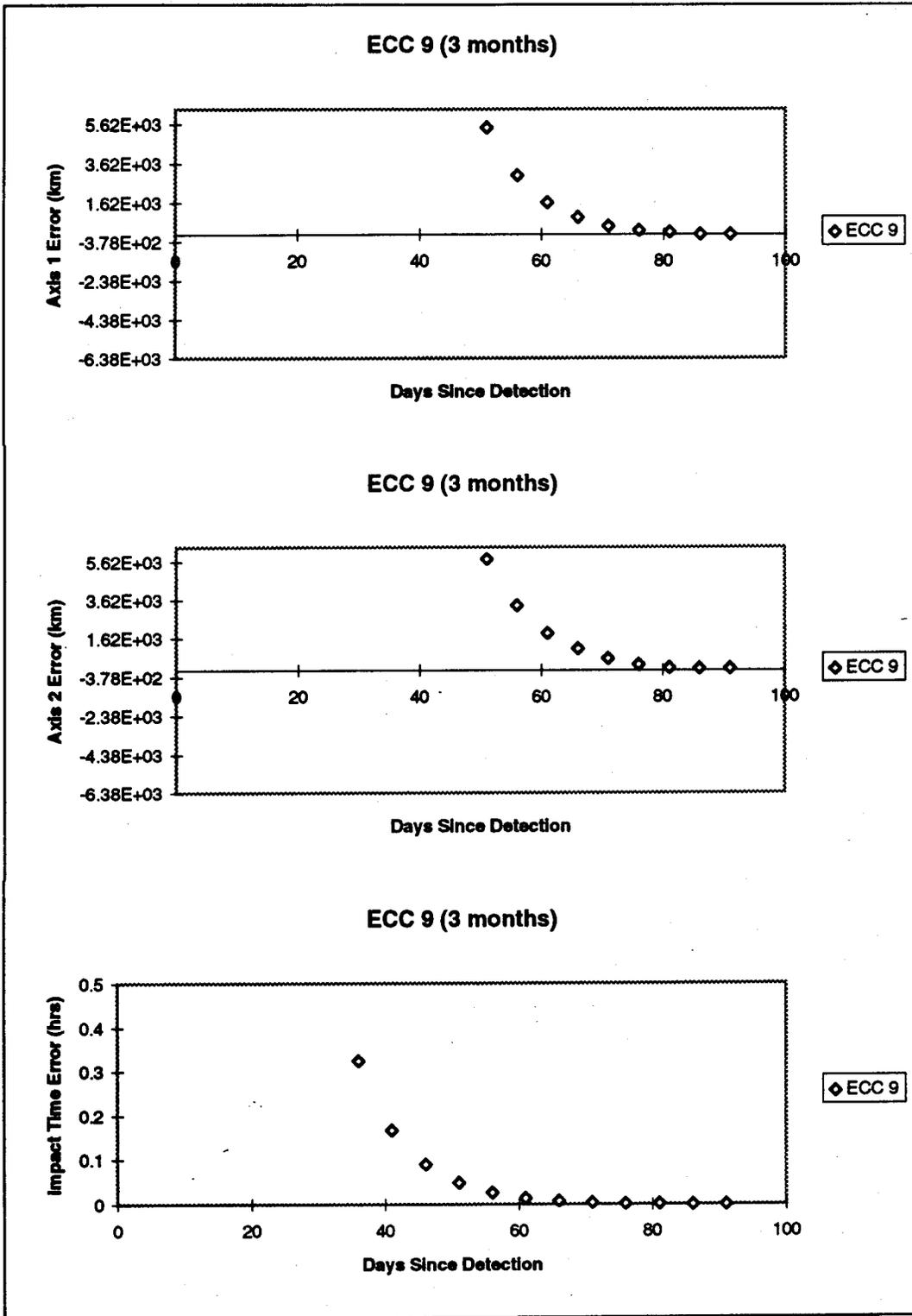
Figure 4.20. Trajectory 9: Simulated Remote Tracking.

TRAJECTORIES 1 and 3 (3 months)

Y (AUs)

2.00E+00
+
0.00E+00 X
X
-2.00E+00
-4.00E+00
-6.00E+00
-8.00E+00
1.00E+01

-5 -4 -3 -2 -1 0 1 2 3

X (AUs)

- ECC 3
O EARTH
X SUN
X EDS 1
+ EDS 2
- ECC 1
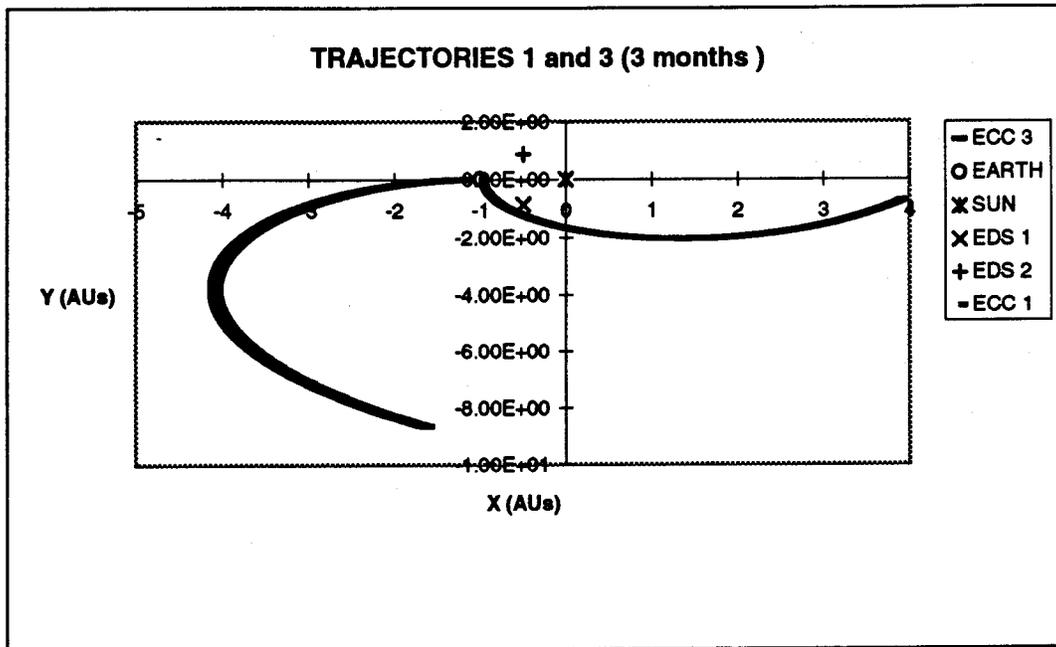
Figure 4.21. Trajectories 1 and 3: Shown with the Proposed EDS Satellites. .

show an overall improvement using obs from all three sources. Still, better overall

estimates were expected when using the combined obs approach. So, hypothesizing that

the results may be hampered by the fact that all of the observation points lay in the same

plane as trajectory 3, the combined ob approach was applied to ECC 1, whose

orbitcontained a "z" component. This type of error is known to occur for some angles-

only estimations when successive obs "lie along the arc of a great circle as viewed from

the observation site" (1:122). This run incorporates 1497 obs over the three months with

the obs taken cumulatively since it was made prior to tripling the observation interval.

Again, all accuracies were 0.1 arcsec. One can see in Figure 4.24 that the combined obs

again represent an improvement and that the results are more consistent. Also, the better

estimates persist longer, particularly for axis one. However, the results are still not nearly

as consistent as with trajectory 9. Also significant is that both error axes are within one

Earth radius only five days following detection, giving 86 days of warning time.

ECC 3 (3 months)

Axis 1 Error (km) vs Days Since Detection

Legend:
▲ ECC 3 (.01 arcsec)
▲ ECC 3 (EDS 1 obs)

ECC 3 (3 months)

Axis 2 Error (km) vs Days Since Detection

Legend:
▲ ECC 3 (.01 arcsec)
▲ ECC 3 (EDS 1 obs)

ECC 3 (3 months)

Impact Time Error (hrs) vs Days Since Detection

Legend:
▲ ECC 3 (.01 arcsec)
▲ ECC 3 (EDS 1 obs)
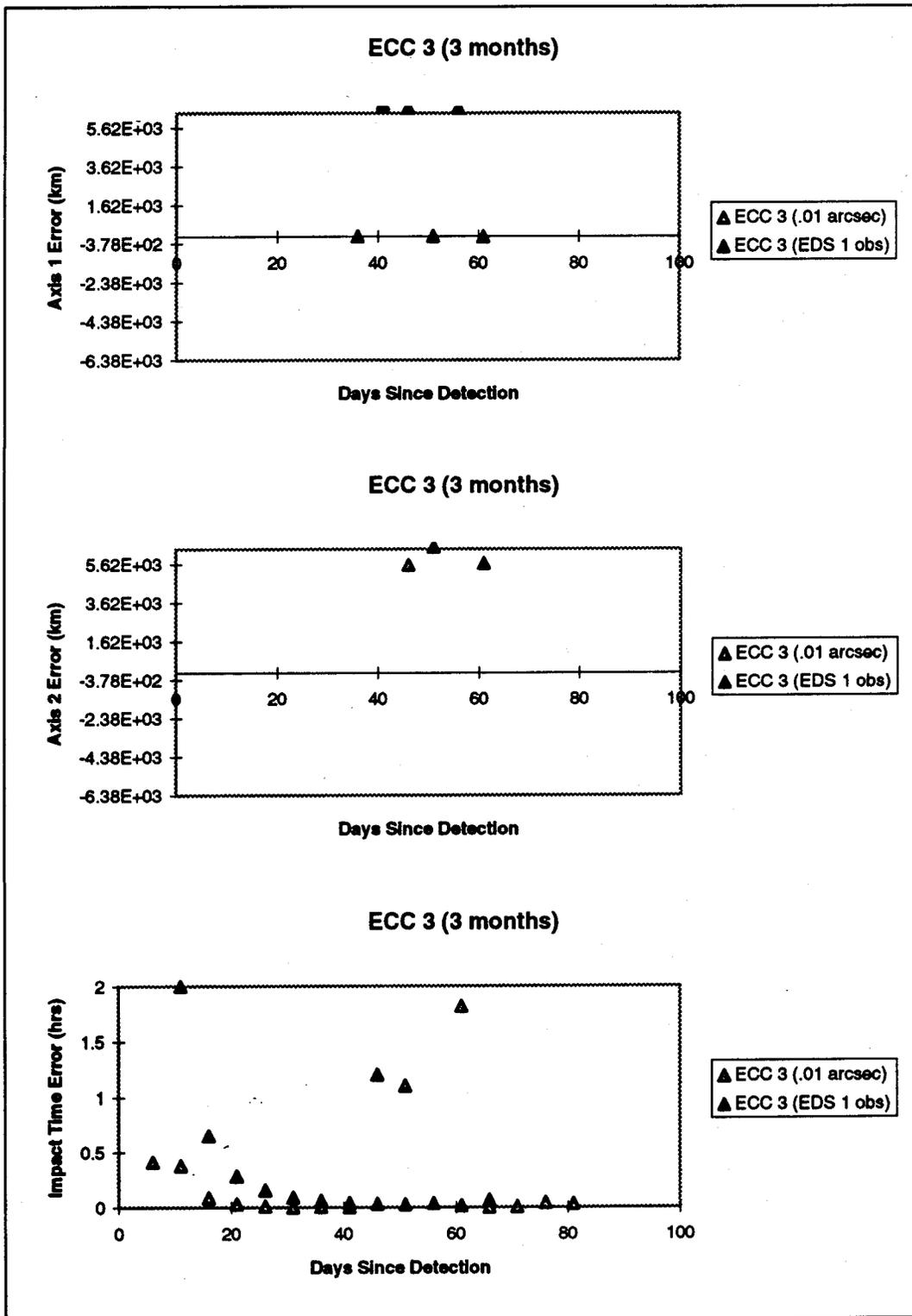
Figure 4.22. Trajectory 3: 0.01 arcsec Accuracy vs. EDS 1 Obs.
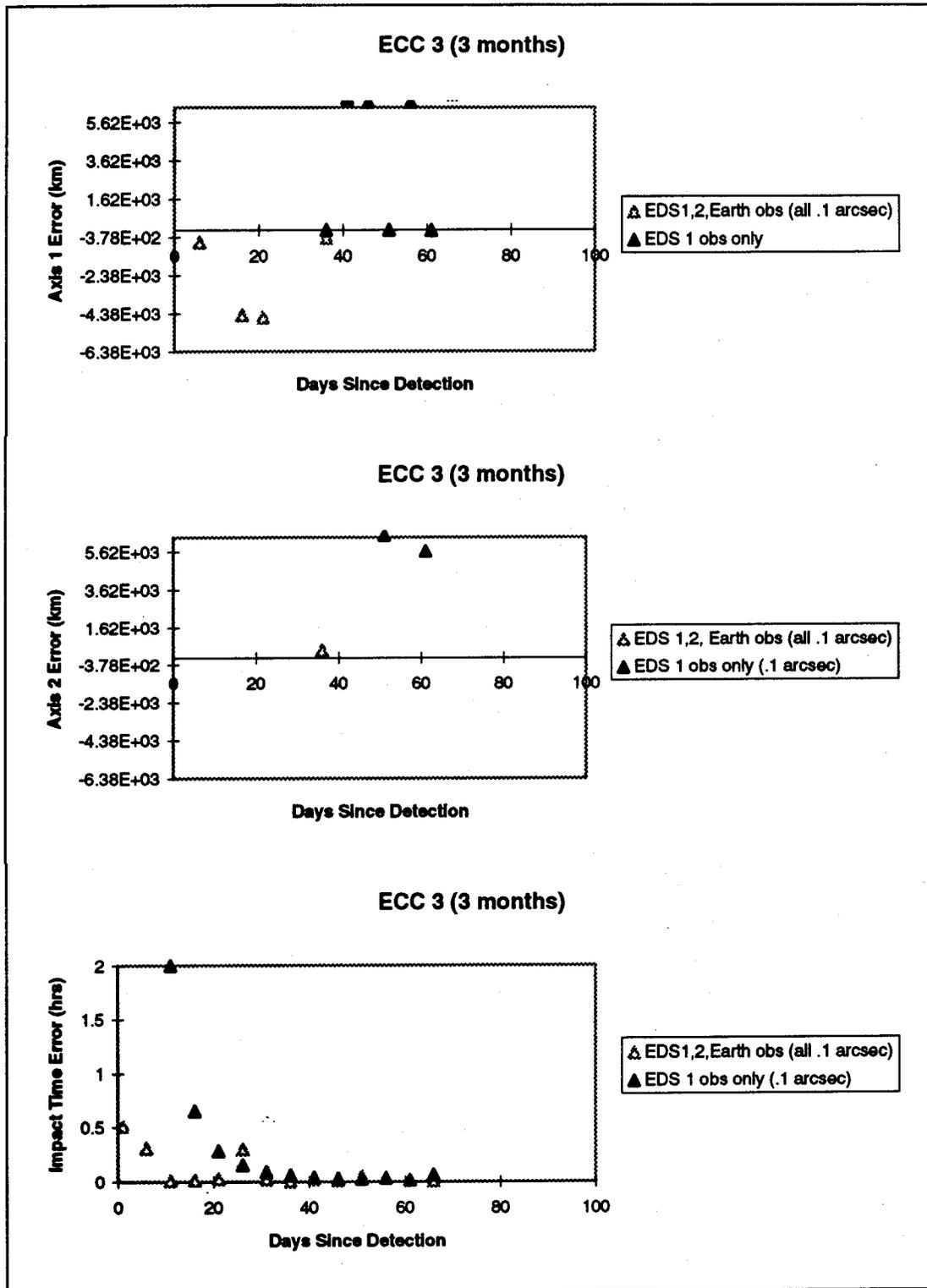
Figure 4.23. Trajectory 3: EDS 1 Obs vs EDS 1, 2, and Earth Obs (all 0.1 arcsec)

ECC 1 (3 months)

Axis 1 Error (km) vs. Days Since Detection

- □ Earth-based obs (.1 arcsec)
- ■ EDS 1,2, Earth obs (all .1 arcsec)

ECC 1 (3 months)

Axis 2 Error (km) vs. Days Since Detection

- □ Earth-based obs (.1 arcsec)
- ■ EDS 1,2, Earth obs (all .1 arcsec)

ECC 1 (3 months)

Impact Time Error (hrs) vs. Days Since Detection

- □ Earth-based obs (.1 arcsec)
- ■ EDS 1,2, Earth obs (all .1 arcsec)
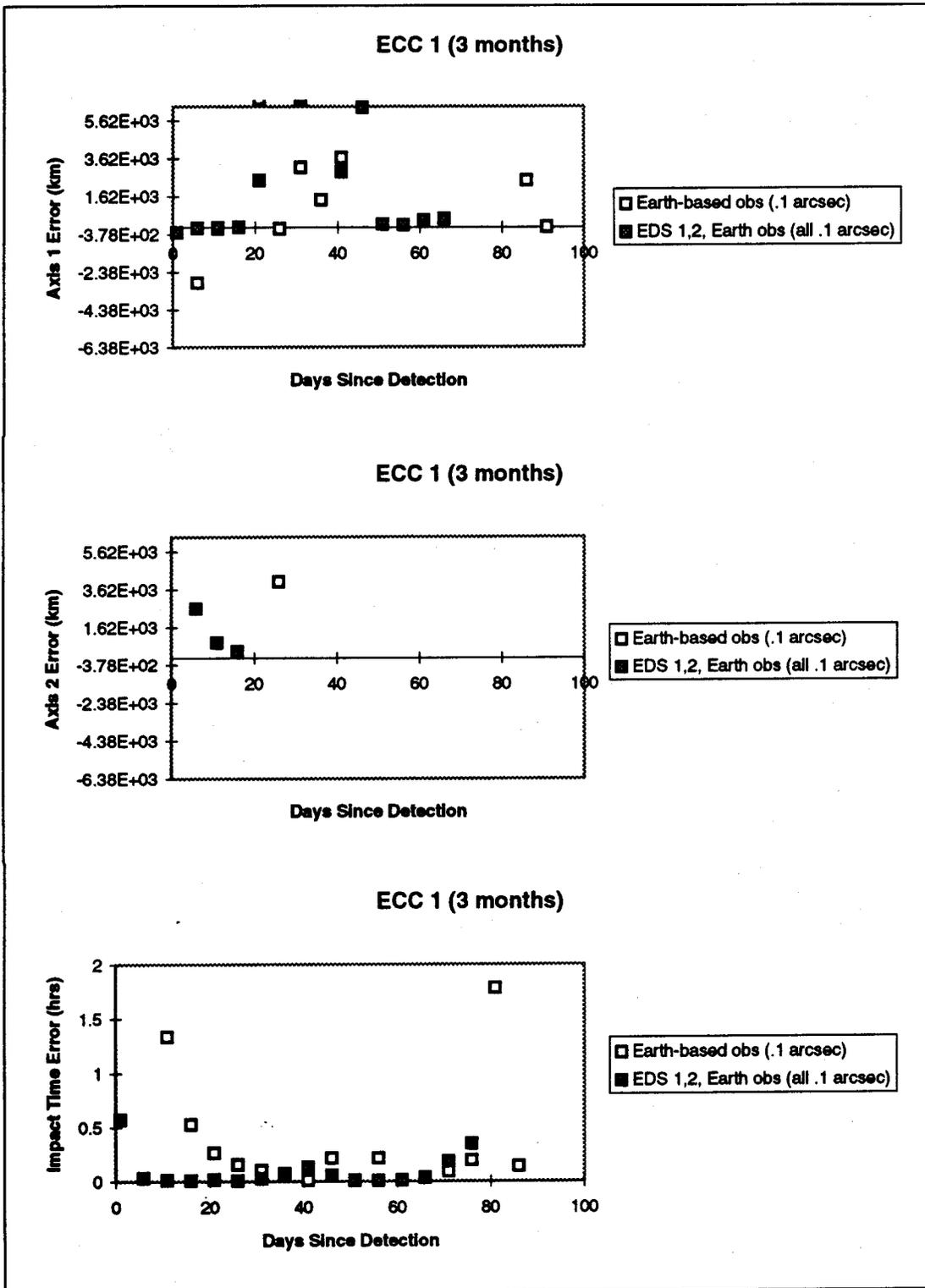
Figure 4.24. Trajectory 1: Baseline vs. EDS 1,2, and Earth Obs

4-24
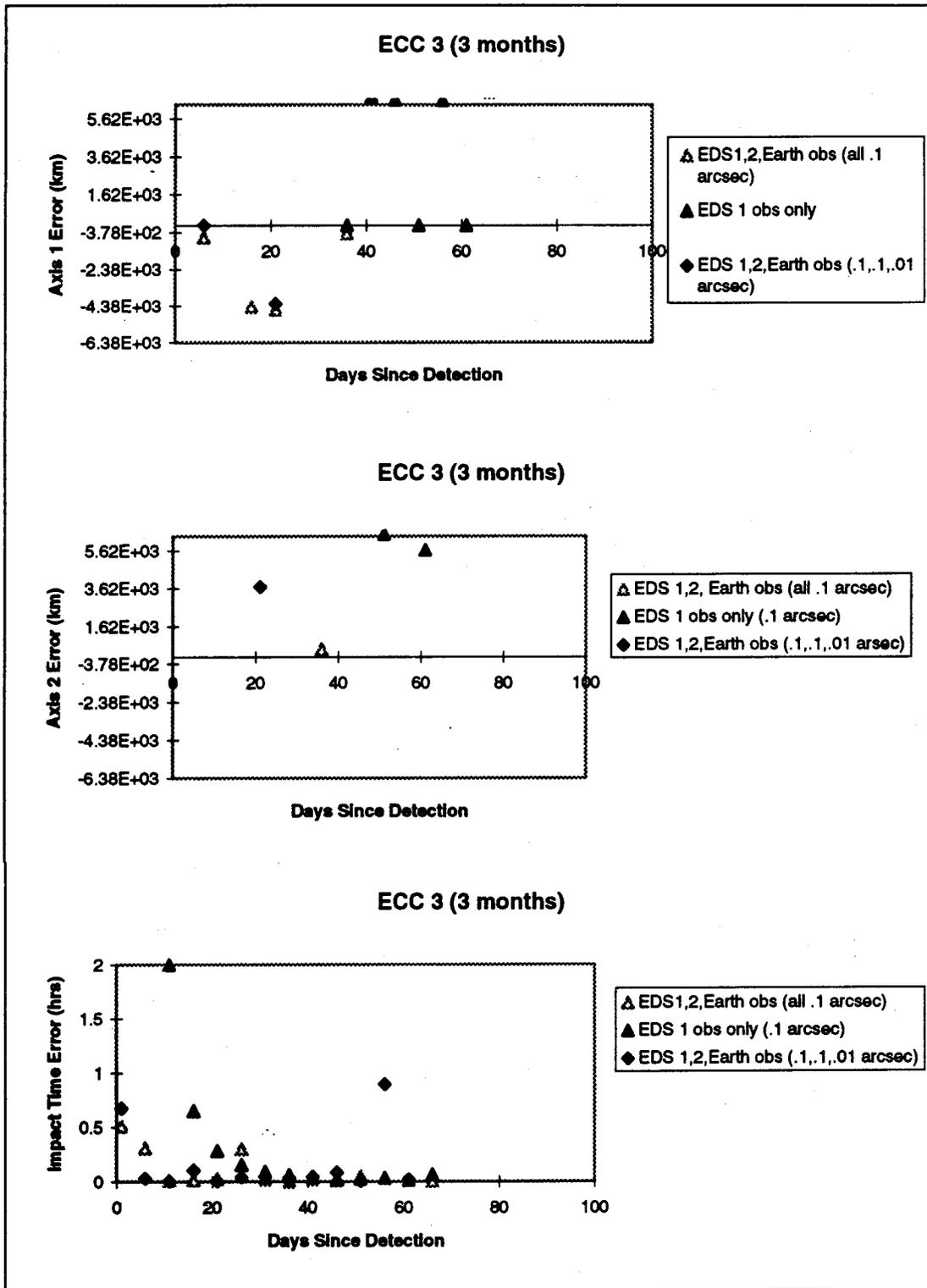
Figure 4.25. Trajectory 3: Comparison of all EDS and Earth-Based Ob Runs

Finally, a run was made to check the effects of using 0.01 arcsec accuracy in place of the 0.1 arcsec for Earth-based obs in the combined estimates. The results for this run are in Figure 4.25. The axis one errors showed little or no improvement but the axis two error was predicted within one Earth radius by day 21, establishing a 15 day advantage over the run with all 0.1 arcsec accuracy.

4.3 Summary of Results.

In order to present a more complete picture at a glance Table 4.1 summarizes the important aspects of the results. First, by looking at the results of the first run for ECC 1, it is obvious, as if we did not know, that we do not want to placed in the position of discovering an ECC just 21 days prior to impact. It took 12 days of observations on ECC 1 just to determine the impact point within one Earth radius. Detecting ECC 1 91 days before impact, however, allowed us to achieve error axes below an Earth radius over two months out with just Earth-based obs at 0.1 arcseconds accuracy. Supplementing these obs with EDS 1 and 2 obs extended this warning to 85 days.

Detecting ECC 2 three months before impact allowed 45 days of warning with only Earth-based observations. Interestingly enough, increasing the amount of observations tenfold offered no real advantage.

ECC 3 proved to be the most challenging trajectory. Therefore it received the most attention. The glaring result, in my mind, from its estimates is they never produced error axes below an Earth radius until EDS obs were used. Although the estimates in the runs which included EDS obs failed to improve with Earth approach, as in the case of ECC 9, they did provide significant warning times and at least one reasonably small error corridor (or box in this case).

ECC 4 offered little information since only the baseline run was made. But it is significant that it, along with ECC 3, established that only 50% of the trajectories could

4-26

be predicted with error axes within an Earth radius using the baseline approach.

Lastly, ECC 9 remains a puzzle when compared to Earth impacting trajectories which incorporated EDS obs. The estimates incorporating EDS obs were expected to be as well behaved. Note, however, that the EDS runs provided better estimates much earlier.

TRAJECTORY	RUN TYPE	EARLIEST BOTH ERROR AXES WITHIN ONE EARTH RADII		SMALLEST ERROR CORRIDOR	
		AXES VALUES(km)	DAYS BEFORE IMPACT	AXES VALUES(km)	DAYS BEFORE IMPACT
ECC1	3 weeks-3612 obs-.1arcsec	60 x 320	9	60 x 320	9
	3 weeks-3612 obs-.01arcsec	0 x 996	5	0 x 996	5
	3 mos-499 obs-.1 arcsec	-83 x 401	65	0 x 99	91
	3 mos-1497 obs-EDS1,2,Earth-.1.1.1arcsec	-70 x 2610	85	4 x 325	16
ECC2	3 mos-499 obs-.1 arcsec	-159 x 4220	45	-75 x 781	20
	3 mos-4990 obs-.1 arcsec	-1210 x 3040	10	-1210 x 3040	10
ECC3	3 mos-499 obs-.1 arcsec	NA	NA	12,100 x 269,000	40
	3 mos-499 obs-.01 arcsec	NA	NA	-20,200 x 5,570	45
	3 mos-499 obs-EDS 1 obs-.1 arcsec	-1 x 6,500 (close)	40	-20 x 5,650	30
	3 mos-499 obs-EDS1,2,Earth obs-.1.1.1 arcsec	-435 x 382	55	-435 x 382	55
	3 mos-499 obs-EDS1,2,Earth obs-.1.1.01 arcsec	-426 x 3,690	70	-426 x 3,690	70
ECC4	3 mos-499 obs-.1 arcsec	NA	NA	2,380 x 81,300	20
ECC9	3 mos-499 obs-.1 arcsec	5,460 x 5,770	40	0 x 80	1

Table 4.1. Summary of Results

V. Conclusions and Recommendations

5.1 Conclusions

I believe that the results presented in Chapter IV, although based on a small sample of possible ECCs, indicate what may be an ominous reality. It appears that, given today's capability, should we detect, on short notice, an ECC which is on a collision course with us, we may not be able to predict its impact with much certainty, until it is within radar range. Angles only observations with 0.1 arcseconds accuracy failed to allow estimates whose one sigma impact footprint was within an Earth radii for two of four ECCs detected 91 days before impact. In addition, varying the amount and accuracy of the observations seemed to offer little or no improvement in the estimates for the two orbits where this was done.

Based on the data for ECC 1, it appears that the task of predicting an impact is particularly difficult if the ECC is detected on very short notice. Having detected ECC 1 21 days before impact, it took 12 of those days to achieve an impact footprint within one Earth radii, leaving little time to avert the collision. For that trajectory, at least, detecting the ECC at 91 days out offered a distinct advantage given only the baseline estimates. I believe, as indicated in Chapter IV, that predicting the orbit of the ECC becomes increasingly difficult as it approaches Earth because of very small angular changes in the trajectory with respect to Earth. The estimates for the non-impacting trajectory, ECC 9, seem to confirm this suspicion since they are much better behaved and continue to improve right down to the "impact" time.

The results obtained when using ECO Detection Satellite observations were mixed. I was disappointed by the fact that those results did not produce the consistent improvement with time that the ECC 9 estimates did. In looking at Figure 4.21, which shows trajectories one and three in relation to the EDSs, I suspect that perhaps the separation between the Earth and the EDSs was too small to alter the geometrical conditions for

trajectories one and three. What I find very encouraging, however, is the increase in warning time provided by the EDS observations. When EDS observations of ECC 1 were fed into the least squares algorithm the one sigma impact footprint fell inside an Earth radii 20 days sooner than with Earth-based obs only. This was achieved with only six days of observations. For ECC 3 the results were even more dramatic. It went from no predictions within an Earth radii, even with increased accuracy, to 40 days warning with EDS 1 obs only. The amount of warning time only increased as EDS 2 obs were added and Earth-based accuracy was improved. I believe that these results alone demonstrate the potential of remote detection of ECCs.

In all of the estimates, the impact time was much more readily predictable. In most cases it could be estimated within minutes or seconds long before impact. This information could be significant in establishing the feasibility of evacuating areas to minimize casualties.

The smallest impact footprint for Earth-impacting ECCs, 0 by 99 km, occurred for ECC 1 using the baseline observations. Unfortunately, this estimate occurred on the day of impact, offering insufficient warning for evacuation purposes. Using EDS obs, the same trajectory was predicted with an error corridor of 4 by 325 km 16 days out. The numbers for the three week run are at least of the same order. Other trajectories offered less promising results, and again, only by using EDS obs could I produce a reasonably small footprint for ECC 3. I believe that these results, along with the impact time estimates, indicate that, depending on the size of the impactor, evacuation may be a possibility.

5.2 Recommendations

Clearly this research should be expanded to sample more possible ECC trajectories. The five orbits which were estimated here may not be representative of a typical one.

Also, further research should include estimating orbits for other types of ECOs. I suspect that estimating the trajectories for objects traveling at half, or less, the speed of the typical ECC should be a less daunting task.

Below are some specific areas which should be addressed:

- Increase the number of estimations with varied accuracy, number of observations, and sources of observations (i.e. remote tracking), perhaps using a monte carlo approach.

- Factor in operational concerns which may prevent observations, such as, weather, opposition by the Sun, and visibility due to site locations.

- Automate the process of building Lstsq input files. This process was extremely time consuming when done manually.

- Investigate our ability to intercept ECOs given angles only data. The error ellipsoids for both an ECC and its interceptor may make this task very challenging.

- Add perturbation effects from other bodies in the solar system and from comet outgassing to the model.

APPENDIX. RAW ERROR DATA

This appendix contains all of the raw error data for axes 1 and 2, as well as impact time errors for each trajectory and run. For days on which no axes or time error data is given, Lstsq failed to converge within 10 iterations. For days on which no time error is given, Lstsq failed to produce an estimate.

Table A.1. Trajectory 1: 3612 obs, 0.1 arcsec, cumulative.

t(days)	axis 1 error (km)	axis 2 error (km)	impact time error (hrs)
1	-1.46E+05	5.18E+06	85.83312114
2	-3.07E+03	7.75E+05	10.82505221
3	-2.83E+02	2.90E+05	3.818209476
4	-6.44E+01	1.10E+05	1.652200285
5	-1.21E+01	4.86E+04	0.723027874
6	2.69E+03	1.90E+05	0.340174697
7	5.44E+05	7.96E+07	3.56E-02
8	4.49E+05	6.83E+07	0.104997883
9	1.52E+04	1.91E+06	5.94E-02
10	1.93E+05	3.86E+07	1.130987148
11	9.69E+05	1.94E+08	0.740125954
12	1.18E+07	2.70E+09	7.912667755
13	2.49E+02	6.71E+04	8.04E-02
14	1.15E+04	2.44E+06	0.131017229
15	7.30E+02	1.63E+05	4.04E-02
16	6.95E+05	1.65E+08	23.19405282
17	5.56E+05	1.20E+08	1.914935887
18	2.41E+05	5.38E+07	1.637294394
19			
20			
21			

Table A.2. Trajectory 1: 3612 obs, 0.1 arcsec, 5 day obspan.

t(days)	axis 1 error (km)	axis 2 error (km)	impact time error (hrs)
1	-1.46E+05	5.18E+06	85.83312114
2	-3.07E+03	7.75E+05	10.82505221
3	-2.83E+02	2.90E+05	3.818209476
4	-6.44E+01	1.10E+05	1.652200285
5	-1.21E+01	4.86E+04	0.723027874
6	-7.01E-02	1.81E+05	0.541404744
7	-3.77E+00	2.69E+04	0.397259613
8	-1.02E+00	2.17E+04	0.247228584
9	4.79E+03	6.00E+05	0.1482692
10	1.35E+03	2.91E+05	4.65E-02
11	-9.48E-03	1.11E+04	8.12E-02
12	-5.92E+01	3.20E+02	0.1657051
13	2.60E+08	3.67E+10	466.5049812
14	6.61E+07	5.97E+09	117.0518521
15	6.49E+07	3.69E+09	338.9855117
16	-5.98E-01	9.61E+03	0.640549955
17	1.48E+06	1.57E+08	56.30452554
18	1.88E+08	1.27E+10	94.00239575
19	-6.42E-03	9.98E+02	9.91E-02
20	-1.82E-03	5.29E+02	6.22E-02
21	-4.79E-02	5.15E+03	1.14726618

Table A.3. Trajectory 1: 3612 obs, 0.01 arcsec, 5 day obspan.

t(days)	axis 1 error (km)	axis 2 error (km)	impact time error (hrs)
1	-1.36E+03	5.04E+05	7.519855736
2	-1.27E+01	1.37E+05	1.229225309
3	1.39E+03	1.62E+05	0.399209666
4	-5.96E-01	1.10E+04	0.161876707
5	2.96E+05	1.05E+08	0.840308621
6	5.59E+04	7.53E+06	1.72E-02
7	2.21E+02	1.77E+04	3.90E-02
8	3.59E+04	9.34E+06	0.402640953
9	3.42E+06	6.72E+08	0.525676002
10	5.79E+03	1.29E+06	3.45E-02
11	1.72E+03	4.01E+05	0.1337857
12	2.67E+08	6.26E+10	25.30085367
13	1.18E+04	2.74E+06	7.49581153
14	6.11E+04	1.10E+07	1.641530119
15	1.11E+06	1.60E+08	11.23719262
16	-6.22E-03	9.96E+02	6.55E-02
17	1.07E+05	2.21E+07	35.1180172
18	8.34E+06	1.32E+09	14.93739406
19	-6.55E-03	1.21E+05	0.488901886
20	-1.09E-04	1.51E+04	8.42E-02
21	9.42E+04	6.72E+07	5.257801322

Table A.4. Trajectory 1: 499 obs, 0.1 arcsec, cumulative.

t(days)	axis 1 error (km)	axis 2 error (km)	impact time error (hrs)
1	-3.94E+07	9.78E+07	711.1462273
6	-2.94E+03	6.45E+05	5.964594853
11	-8.85E+01	1.62E+05	1.331626424
16	1.40E+04	2.58E+05	0.524848604
21	6.79E+03	1.38E+05	0.260750339
26	-8.28E+01	4.01E+03	0.15359081
31	3.13E+03	3.25E+05	9.78E-02
36	1.44E+03	1.09E+05	6.75E-02
41	3.67E+03	6.70E+05	1.17E-02
46	1.92E+04	3.02E+06	2.13E-01
51	1.82E+04	2.72E+06	2.97E-03
56	1.45E+04	2.52E+06	2.14E-01
61	3.63E+04	5.68E+06	9.24E-03
66	2.01E+04	3.25E+06	3.25E-02
71	2.26E+04	3.89E+06	8.95E-02
76	1.09E+05	2.00E+07	1.93E-01
81	8.66E+06	1.85E+09	1.78E+00
86	2.46E+03	5.48E+05	1.41E-01
91	-3.58E-06	1.99E+03	1.48E-02

Table A.5. Trajectory 1: 1497 obs, EDS 1, 2, Earth-based, 0.1 arcsec, cumulative.

t(days)	axis 1 error (km)	axis 2 error (km)	impact time error (hrs)
1	-2.86E+02	6.44E+04	0.569164981
6	-7.03E+01	2.61E+03	3.05E-02
11	-3.86E+01	8.01E+02	1.15E-02
16	-4.01E+00	3.25E+02	6.21E-03
21	2.45E+03	5.35E+05	1.45E-02
26	9.14E+03	2.00E+06	2.70E-03
31	6.72E+03	1.50E+06	2.66E-02
36	1.93E+04	4.28E+06	6.45E-02
41	2.93E+03	6.40E+05	0.129517642
46	6.32E+03	1.40E+06	5.44E-02
51	1.55E+02	3.75E+04	8.40E-03
56	1.27E+02	3.08E+04	5.93E-03
61	3.38E+02	7.52E+04	8.14E-03
66	4.16E+02	9.45E+04	3.05E-02
71	7.41E+03	1.72E+06	1.81E-01
76	7.17E+04	1.76E+07	3.47E-01
81			
86			
91			

Table A.6. Trajectory 2: 499 obs, 0.1 arcsec, 5 day obspan.

t(days)	axis 1 error (km)	axis 2 error (km)	impact time error (hrs)
1			
6	1.85E+08	3.53E+08	254.769505
11			
16	-1.09E+09	3.79E+08	1042.453575
21	2.61E+09	4.34E+09	3669.476954
26	4.13E+08	8.60E+08	1177.11037
31	-3.91E+07	9.88E+07	141.8964258
36	-2.52E+07	6.93E+07	113.5889355
41	-9.86E+06	4.70E+07	42.44353565
46	-6.98E+06	3.19E+07	35.74990059
51	-2.17E+06	1.07E+07	37.92006361
56	-1.16E+06	6.26E+06	28.27082651
61	-1.34E+05	9.74E+05	18.4948707
66	-1.99E+04	1.79E+05	10.68506267
71	2.71E+05	1.27E+06	3.582850588
76	3.16E+05	1.20E+06	2.216469271
81	1.49E+04	4.82E+05	4.33E-03
86	2.29E+04	2.10E+05	1.68E-02
91	1.73E+04	2.98E+05	1.32E-02

Table A.7. Trajectory 2: 499 obs, 0.1 arcsec, cumulative.

t(days)	axis 1 error (km)	axis 2 error (km)	impact time error (hrs)
1	-5.64E+15	2.05E+10	
6			
11	-1.84E+07	7.94E+07	108.1549043
16	-1.23E+06	9.05E+06	40.20441933
21	-7.00E+04	3.10E+06	8.244635813
26	-7.00E+04	3.10E+06	8.244635813
31	-1.50E+03	4.10E+05	1.20541914
36	-4.54E+02	1.83E+05	0.543311731
41	-9.91E+01	8.48E+04	0.258333382
46	-1.59E+02	4.22E+04	1.32E-01
51	-1.83E+02	2.09E+04	6.89E-02
56	-1.51E+03	1.06E+04	3.92E-02
61	-3.30E+02	5.07E+03	2.10E-02
66	-4.77E+02	2.07E+03	1.40E-02
71	-7.48E+01	7.81E+02	7.21E-03
76	3.69E+02	2.31E+04	5.66E-03
81	2.70E+05	6.04E+07	1.26E-01
86	4.13E+04	8.96E+06	4.52E-01
91	1.15E+05	2.59E+07	6.23E-02

Table A.8. Trajectory 2: 4990 obs, 0.1 arcsec, 5 day obspan.

t(days)	axis 1 error (km)	axis 2 error (km)	impact time error (hrs)
1	1.13E+09	2.55E+10	5090.315638
6	5.86E+09	1.01E+10	432.5819693
11	3.99E+07	1.95E+08	1158.478344
16	5.62E+07	2.49E+08	67.96201072
21	2.94E+07	1.07E+08	49.82817551
26	-9.45E+06	5.56E+07	67.21223945
31	-5.02E+06	2.85E+07	60.57775601
36	-3.50E+09	1.04E+07	72.43164536
41	-1.19E+06	1.02E+07	30.56646504
46	-5.52E+05	6.48E+06	19.17285621
51	-2.24E+05	2.89E+06	14.6393481
56	-9.23E+04	1.63E+06	8.876391656
61	-1.97E+04	4.38E+05	5.984089461
66	-1.08E+03	4.21E+04	3.154395798
71	8.12E+04	4.16E+05	1.23E+00
76	9.37E+04	3.93E+05	6.34E-01
81	-1.21E+03	3.04E+03	2.96E-03
86	1.42E+08	3.16E+10	13.7865782
91	1.16E+05	3.30E+07	6.87E-02

Table A.9. Trajectory 3: 499 obs, 0.1 arcsec, 5 day obspan.

t(days)	axis 1 error (km)	axis 2 error (km)	impact time error (hrs)
1	-1.86E+22	-1.41E+21	
6	4.84E+08	9.57E+08	29.7592837
11			
16	8.76E+08	1.48E+09	33.04819083
21			
26	6.57E+08	7.39E+08	29.2698303
31	6.51E+08	1.29E+09	28.45676243
36	6.88E+08	1.29E+09	24.73305934
41	1.27E+10	2.26E+10	45.28532194
46	1.83E+11	3.05E+11	109.5737957
51	3.82E+08	5.90E+08	6.496341447
56	4.14E+08	5.90E+08	5.098399626
61	4.96E+08	3.68E+09	58.90742388
66	1.71E+08	1.92E+08	1.261983226
81	5.62E+07	7.09E+07	6.82E-03
86	4.00E+07	2.45E+08	1.323892526
91			

Table A.10. Trajectory 3: 499 obs, 0.1 arcsec, cumulative.

t(days)	axis 1 error (km)	axis 2 error (km)	impact time error (hrs)
1	-1.86E+22	-1.41E+21	
6	-1.58E+05	1.52E+08	5.099635407
11	5.71E+07	1.20E+08	4.438662699
16	1.78E+07	2.82E+07	0.782285087
21	5.79E+06	1.02E+07	0.287279927
26	2.69E+06	4.47E+06	0.112243726
31	1.33E+06	2.21E+06	4.26E-02
36	7.43E+05	1.22E+06	5.45E-02
41	4.33E+05	7.03E+05	2.09E-03
46	3.17E+05	4.32E+05	2.45E-02
51	-1.21E+04	2.69E+05	1.68E-02
56	1.78E+05	2.42E+06	1.25E-02
61	9.02E+06	1.11E+09	3.20E+01
66	7.92E+04	6.90E+05	5.17E-04
71	1232938	211973000	0.094262985
76	4.03E+06	7.10E+08	1.204137223
81	6.07E+08	8.43E+10	70.7513739
86	7.29E+06	1.04E+09	7.565157248
91			

Table A.11. Trajectory 3: 499 obs, 0.01 arcsec, cumulative.

t(days)	axis 1 error (km)	axis 2 error (km)	impact time error (hrs)
1	-1.50E+17	-1.76E+16	
6	9.30E+07	1.33E+08	0.413282491
11	6.25E+06	1.13E+07	0.375497987
16	1.65E+06	2.87E+06	8.51E-02
21	6.24E+05	1.01E+06	2.79E-02
26	2.61E+05	4.50E+05	1.19E-02
31	1.63E+05	2.22E+05	1.97E-03
36	-9.16E+04	1.04E+05	4.46E-03
41	7.08E+04	4.40E+05	1.72E-03
46	-2.02E+04	5.57E+03	1.20E+00
51	9.65E+05	1.47E+08	1.10E+00
56	1.61E+07	3.91E+09	1.54E+01
61	8.42E+06	1.68E+09	1.82E+00
66	1.09E+05	2.60E+07	1.76E-03
71	9.50E+04	2.01E+07	4.26E-03
76	8.80E+04	1.88E+07	4.10E-02
81	6.08E+04	1.24E+07	3.08E-02
86	5.78E+06	1.20E+09	2.93E+00
91			

Table A.12. Trajectory 3: 499 EDS 1 obs, 0.1 arcsec, cumulative.

t(days)	axis 1 error (km)	axis 2 error (km)	impact time error (hrs)
1			
6	5.78E+07	9.07E+07	13.24252676
11	4.50E+06	7.39E+06	1.999696328
16	9.75E+05	1.76E+06	0.649874058
21	2.71E+05	5.78E+05	0.28498069
26	9.15E+04	2.04E+05	0.151914622
31	3.10E+04	5.86E+04	8.98E-02
36	-1.18E+01	1.15E+04	5.87E-02
41	6.85E+03	1.48E+04	4.03E-02
46	6.66E+03	3.40E+04	2.97E-02
51	-9.01E-01	6.50E+03	2.26E-02
56	6.65E+03	2.41E+05	3.31E-02
61	-2.03E+01	5.65E+03	1.57E-02
66	8.12E+04	1.93E+07	6.39E-02
71			
76			
81			
86			
91			

Table A.13. Traj 3: 1497 EDS 1, 2, & Earth-based obs, 0.1 arcsec, cumulative.

t(days)	axis 1 error (km)	axis 2 error (km)	impact time error (hrs)
1	1.93E+06	3.23E+06	0.350973807
6	-1.07E+03	9.66E+04	8.94E-02
11	-3.56E+01	3.38E+04	2.60E-02
16	1.70E+04	5.41E+05	3.12E-02
21	1.37E+04	3.71E+06	5.49E-02
26	4.35E+04	9.51E+06	8.02E-03
31	3.19E+04	6.99E+06	3.18E-02
36	8.97E+04	2.04E+07	8.50E-02
41	5.31E+04	1.21E+07	1.04E+00
46	2.28E+04	5.10E+06	3.63E-02
51	6.81E+04	1.55E+07	1.14E-01
56	1.97E+04	4.36E+06	4.55E-03
61	2.00E+05	4.47E+07	4.75E-01
66	3.93E+03	8.44E+05	2.96E-03
71			
76			
81			
86			
91			

Table A.14. Traj 3: 499 EDS 1, 2, & Earth-based obs, 0.1 arcsec, cumulative.

t(days)	axis 1 error (km)	axis 2 error (km)	impact time error (hrs)
1	2.58E+06	2.86E+06	0.50959139
6	-6.58E+02	1.68E+05	3.08E-01
11	5.87E+04	1.18E+05	1.21E-02
16	-4.45E+03	2.90E+04	1.71E-02
21	-4.57E+03	1.54E+04	2.72E-02
26	2.20E+05	4.58E+07	2.96E-01
31	8.04E+03	7.89E+05	1.97E-02
36	-4.35E+02	3.82E+02	4.43E-04
41	1.79E+04	3.57E+06	2.16E-02
46	1.47E+04	3.13E+06	8.14E-03
51	3.10E+04	6.96E+06	4.98E-02
56	1.57E+04	3.33E+06	2.73E-02
61	1.05E+04	2.26E+06	1.43E-02
66	7.06E+03	1.53E+06	2.97E-03
71			
76			
81			
86			
91			

Table A.15. Traj 3: 499 EDS 1, 2, & Earth-based obs, 0.1, 0.1, & 0.01 arcsec, cum.

t(days)	axis 1 error (km)	axis 2 error (km)	impact time error (hrs)
1	1.54E+06	1.74E+06	0.674528912
6	-5.56E+00	1.03E+05	2.79E-02
11	3.58E+04	3.80E+05	4.34E-03
16	1.74E+05	3.35E+07	1.02E-01
21	-4.26E+03	3.69E+03	6.15E-03
26	8.70E+04	1.70E+07	3.85E-02
31	4.99E+04	9.93E+06	4.29E-02
36	3.55E+04	7.41E+06	3.64E-02
41	2.70E+04	5.78E+06	4.22E-02
46	1.28E+05	2.97E+07	8.61E-02
51	1.67E+04	3.67E+06	6.42E-03
56	3.32E+06	7.42E+08	8.92E-01
61	1.11E+04	2.43E+06	2.07E-02
66	4.69E+08	1.08E+11	6.74E+00
71			
76			
81			
86			
91			

Table A.16. Trajectory 4: 499 obs, 0.1 arcsec, cumulative.

t(days)	axis 1 error (km)	axis 2 error (km)	impact time error (hrs)
1	-1.62E+26	-1.17E+26	
6	9.86E+06	1.24E+07	177.4958311
11	-6.06E+03	5.03E+05	35.86787693
16	4.88E+04	3.42E+05	10.67176713
21	1.32E+04	3.74E+04	4.534903195
26	1.46E+04	1.40E+05	2.358488096
31	1.16E+04	1.38E+05	1.37E+00
36	8.91E+03	1.67E+05	8.76E-01
41	7.34E+03	1.14E+05	5.88E-01
46	5.94E+03	1.98E+05	4.22E-01
51	4.89E+03	2.51E+05	3.14E-01
56	2.31E+04	3.15E+06	3.29E-01
61	4.25E+03	4.24E+05	2.12E-01
66	1.07E+04	2.12E+06	4.13E-01
71	2382.292	81259.94	0.150697734
76	8.41E+04	1.97E+07	1.5706099
81	1.43E+04	4.40E+06	0.120631884
86	4.61E+06	1.12E+09	1.335231893
91	6.70E+08	1.97E+11	130.7675316

Table A.17. Trajectory 9: 499 obs, 0.1 arcsec, cumulative.

t(days)	axis 1 error (km)	axis 2 error (km)	impact time error (hrs)
1	-1.50E+22	3.65E+15	97324.73375
6	4.39E+07	4.70E+07	325.9593788
11	3.29E+06	4.03E+06	39.32366484
16	8.87E+05	1.03E+06	9.818091482
21	3.09E+05	3.54E+05	3.335262997
26	1.36E+05	1.51E+05	1.405861805
31	6.44E+04	7.00E+04	0.642927528
36	3.37E+04	3.57E+04	0.323745214
41	1.81E+04	1.85E+04	0.166267293
46	1.01E+04	1.02E+04	8.98E-02
51	5.46E+03	5.77E+03	4.81E-02
56	3.02E+03	3.35E+03	2.64E-02
61	1.61E+03	1.90E+03	1.41E-02
66	8.53E+02	1.08E+03	7.47E-03
71	4.20E+02	5.80E+02	3.72E-03
76	1.94E+02	2.81E+02	1.72E-03
81	9.17E+01	1.01E+02	7.38E-04
86	-4.87E-05	8.11E+01	3.04E-04
91	-5.11E-05	8.03E+01	2.13E-04

Bibliography

1. Bate, Roger R., Donald D. Mueller, and Jerry E.White. <u>Fundamentals of Astrodynamics</u>. New York: Dover Publications, Inc., 1971.

2. Browne, Malcolm W. "Great Balls of Fire," <u>The Grand Forks Herald</u>, 20 July 1994, sec A:1.

3. Caravan, Gregory H., Johndale C. Solem, and John D. G. Rather, eds. <u>Proceedings of the Near-Earth-Object Interception Workshop</u>. LA-12476-C Conference (Los Alomos, NM: Los Alamos National Laboratories, Feb 1993), 233.

4. Chapman, Clark R., and David Morrison. "Impacts on the Earth by asteroids and comets: assessing the hazard," <u>Nature, volume 367</u>: 33-39 (6 January 1994).

5. Department of the Air Force. "Preparing for Planetary Defense: Detection and Interception of Asteroids on Collision Course with Earth," AU-White Paper. Maxwell AFB, Alabama: Air University Press, 1994.

6. Hills, Jack G. and M. P.Goda. "The Fragmentation of Small Asteroids in the Atmosphere", <u>Astronomical Journal</u>: 1114-1144 (March 1993).

7. Maryniak, Gregg E., "Improving the Detection of Near-Earth-Asteroids," Space Studies Institute, Princeton, N.J.: 1992.

8. Morrison, David, editor. "The Spaceguard Survey: Report of the Near-Earth-Object Detection Workshop," (January 1992).

9. Pope, Gregory T., contributing editor. "When Worlds Collide," <u>Popular Mechanics</u>: 106, (March 1994).

10. Shaffer, William A., Martin J. McHugh, and Dexter Wang. "Asteroid Detection and Monitoring Using a Satellite-Borne Visible Scanner," Naval Research Laboratory, Washington, D.C.: 1993.

11. Szebehely, Victor. <u>Theory of Orbits: The Restricted Problem of Three Bodies</u>. New York: Academic Press, 1967.

12. Wiesel, William E. <u>Spaceflight Dynamics</u>. New York: McGraw-Hill, Inc. 1989.

13. Wiesel, Dr. William E., Data Simulator/Least Squares Estimation
    FORTRAN Library Units, School of Engineering, Air Force Institute of Technology
    (AU), Wright-Patterson AFB, OH, 1 OCT 1994.

14. Wiesel, Dr. William E., Class notes for MECH 636, Advanced
    Astrodynamics, School of Engineering, Air Force Institute of Technology (AU),
    Wright-Patterson AFB OH, April 1994.

15. Wiesel, Dr. William E., Class notes for MECH 731, Modern Methods of
    Orbit Determination, School of Engineering, Air Force Institute of Technology (AU),
    Wright-Patterson AFB OH, June 1994.

16. Yeomans, D.K., et al. "Asteroid and Comet Orbits Using Radar Data",
    Astronomical Journal: 303-317 (January 1992).

VITA

Captain Gregory A. Bishop was born on 27 March 1963 in Cincinnati, Ohio. He graduated from Norwood High School in Norwood, Ohio in 1981 and entered Miami University. In 1982 he enrolled in the Air Force ROTC program and in May 1985 graduated with a Bachelor of Science in Aeronautics. Upon graduation he received his commission as a Second Lieutenant and attended Space Operations Training at the 3400th Technical Training Wing, Lowry AFB, Colorado. He was assigned to the 4th Satellite Communications Squadron, Holloman AFB, New Mexico until January 1990. While there, he served as a Space Systems Crew Commander, line crew instructor, Field Commander, and Flight Commander for this one of a kind mobile Air Force Space Command unit. He attended Squadron Officer School in residence from January to March 1990 while enroute to his next assignment at the 1st Command and Control Squadron, Cheyenne Mountain AFB, Colorado. There he served as a Space Surveillance Crew Commander, Chief of Operations Training, Chief of Space Surveillance Center Operations, and line crew evaluator until April 1993. It was during this time that Captain Bishop was selected to attend the Air Force Institute of Technology (AFIT) to pursue a Master's Degree in Space Operations. Captain Bishop entered AFIT's School of Engineering in May 1993. He has a wife and three children.

Permanent Address: 5700 Melody Lane
Milford, OH 45150

REPORT DOCUMENTATION PAGE

1. AGENCY USE ONLY (Leave blank)	2. REPORT DATE December 1994	3. REPORT TYPE AND DATES COVERED Master's Thesis

4. TITLE AND SUBTITLE

Tracking and Impact Prediction of Earth-Crossing-Objects (ECOs) on a Collision Course with Earth

5. FUNDING NUMBERS

6. AUTHOR(S)

Gregory A. Bishop, Capt, USAF

7. PERFORMING ORGANIZATION NAME(S) AND ADDRESS(ES)

Air Force Institute of Technology, WPAFB, OH 45433-6583

8. PERFORMING ORGANIZATION REPORT NUMBER

AFIT/GSO/ENY/94D-01

9. SPONSORING / MONITORING AGENCY NAME(S) AND ADDRESS(ES)

10. SPONSORING / MONITORING AGENCY REPORT NUMBER

11. SUPPLEMENTARY NOTES

12a. DISTRIBUTION / AVAILABILITY STATEMENT

Approved for Public Release; Distribution Unlimited

12b. DISTRIBUTION CODE

13. ABSTRACT *(Maximum 200 words)*

This study investigated the effectiveness of Earth-based angles only observations in determining the orbit of various hypothetical Earth-Crossing-Objects (ECOs). "True" trajectories were simulated specifically for Earth-Crossing-Comets (ECCs) by numerically integrating in a Restricted Three Body system. Starting at Earth impact points, the state vectors were "reverse-propagated" to a proposed detection time. Observations (obs), with state-of-the-art accuracy, were then simulated with error induced by a Gaussian random number generator; these were used in a least-squares differential corrector to estimate the positions of the ECOs. State vectors and covariance matrices were then propagated to the impact times and axis lengths of the one sigma impact footprint were calculated. Varied amounts of data were fed into the differential corrector and it was determined that Earth-based obs alone may be ineffective in predicting an ECC's orbit.

14. SUBJECT TERMS

Asteroids, Comets, Orbit Determination Differential Correction, Impact Prediction

15. NUMBER OF PAGES

101

16. PRICE CODE

17. SECURITY CLASSIFICATION OF REPORT	18. SECURITY CLASSIFICATION OF THIS PAGE	19. SECURITY CLASSIFICATION OF ABSTRACT	20. LIMITATION OF ABSTRACT
UNCLASSIFIED	UNCLASSIFIED	UNCLASSIFIED	UL